DISCRIMINATING THE PRODUCTS OF ALLOGENIC FORCINGS

AND AUTOGENIC PROCESSES

FROM SEDIMENT SOURCES TO SINKS

A DISSERTATION SUBMITTED ON THE NINETEENTH DAY OF AUGUST 2016

TO THE DEPARTMENT OF EARTH AND ENVIRONMENTAL SCICENCES

IN PARTIAL FULFILLMENT OF THE REQUREMENTS

OF THE SCHOOL OF SCIENCE AND ENGINEREERING

OF TULANE UNIVERSITY FOR THE DEGREE OF

DOCTOR OF PHILOSOPHY

BY

_____

(QI LI)

APPROVED: _____

Kyle M. Straub, Ph.D., Director

_____

Nicole M. Gasparini, Ph.D.

_____

Torbjörn E. Törnqvist, Ph.D.

_____

Elizabeth Hajek, Ph.D.

ABSTRACT

Sedimentary deposits contain the most complete records of paleo-environmental signals over the greatest fraction of Earth's history (Blum and Törnqvist, 2000; Paola, 2000; Paola et al., 2009; Romans et al., 2015). Unfortunately, we lack tools to accurately extract these paleo-environmental signals from stratigraphy, partially due to stochastic processes internal to sediment transport systems that occur along a source to sink path. To overcome this, I utilize reduced scale laboratory experiments, numerical modelling and statistical methods to discriminate the products of environmental forcings and internal (autogenic) processes in both erosional and depositional settings. This thesis includes three major chapters. In the first major chapter, I conduct a series of numerical experiments to explore how changes in rock uplift rate translate into sediment flux signals at the outlet of erosional landscapes. I find that rock uplift rate changes with short duration likely do not translate into sediment flux signals at the outlet of erosional landscapes. Once sediment is produced in the erosional engine, properties of the sediment flux, such as sediment cohesion, influence the temporal and spatial scales of autogenic processess in sedimentary sytems and the stratigraphic record. To differeniate the stratigraphic products of autogenic processes and allogenic forcings, I use physical experiments to quantify how sediment cohesion influences the architecture of stratigraphy over a basin filling time scales. I observe that an increase in sediment cohesion decreases lateral channel mobility, which increases the temporal and spatial persistence of stratigraphic trends. In addition, sediment cohesion decreases the volume of channel relative to overbank

and marine deposits and the segregation of fine from coarse material in stratigraphy. In the last chapter, I use physical experiments and statistical methods to define the storage thresholds of Relative Sea Level (RSL) signals in the stratigraphic record. I find that RSL cycles with magnitudes and periodicities less than the spatial and temporal scales of the internal (autogenic) dynamics of deltas cannot confidently be extracted from the physical stratigraphic record. Combined, the results in this thesis advance our capacity to invert stratigraphic records for paleo-environmental history and forward model the evolution of sediment transport systems and their stratigraphic products.

DISCRIMINATING THE PRODUCTS OF ALLOGENIC FORCINGS

AND AUTOGENIC PROCESSES

FROM SEDIMENT SOURCES TO SINKS

AN ABSTRACT SUBMITTED ON THE NINETEENTH DAY OF AUGUST 2016

TO THE DEPARTMENT OF EARTH AND ENVIRONMENTAL SCICENCES

IN PARTIAL FULFILLMENT OF THE REQUREMENTS

OF THE SCHOOL OF SCIENCE AND ENGINEREERING

OF TULANE UNIVERSITY FOR THE DEGREE OF

DOCTOR OF PHILOSOPHY

BY

_____

(QI LI)

APPROVED: _____

Kyle M. Straub, Ph.D., Director

_____

Nicole M. Gasparini, Ph.D.

_____

Torbjörn E. Törnqvist, Ph.D.

_____

Elizabeth Hajek, Ph.D.

ACKNOWLEGEMENTS

First and foremost, I would like to express my special appreciation and thanks to my advisor Professor Kyle M. Straub. He is one of the most hardworking and smartest persons I know. It has been my honor to work with him. He not only sets an excellent example of being a good scientist and mentor for me, but also provides me with numerous wise guidance and insightful advices on my research and career. I really appreciate all his contributions of time, ideas and funding to make my Ph.D. experience productive and exciting. At the same time, I would also thank Professor Nicole M. Gasparini for her smart guidance on my second project and countless encouragement. She has been actively interested in my research and always patiently answering my questions. She always encourages me when I meet difficulty in my research and life. I really appreciate her guidance and help. I also want to thank Professor Torbjörn E. Törnqvist and Elizabeth Hajek for serving my thesis committee and giving me numerous inspirational advices on my thesis. It is my pleasure to work with so many knowledgeable and supportive professors. Without guidance and constant feedback from my four thesis committee members, this thesis would not have been achievable.

I also want to extend my gratitude to all current and past lab members, Lizhu Yu, Christopher Esposito, Tushar Bishnoi, Matthew Benson, Anjali Fernandes, Diana Di Leonardo, Yinan Wang and Jennifer Kuykendall. Whenever I have difficulty in my life and research, they always encourage me and provide me with numerous

thoughtful suggestions. Without their help, I could not have finished the five laboratory experiments for the data collection of my thesis.

I also want to thank my parents and friends for their immeasurable encouragement and help. My parents and other family members always support my in all my pursuits. Words cannot express how grateful I am to them for all sacrifice that they have made on my behalf. For my friends, Yuanzhen Cheng, Yueheng Zhang, Bowen Shi, Haixing Wang, Yan Ren, Siyuan Jiang, Yixuan Li, they are always supportive to me and make my life fun and vivid.

TABLE OF CONTENTS

LIST OF FIGURES

LIST OF TABLES

Chapter 1

Introduction

Autogenic dynamics (Beerbower, 1961; Slingerland and Smith, 2004; Paola, In Press), such as river avulsion and lobe switching, are often regarded as noise in sediment transport systems, compared to the temporal and spatial scales of allogenic forcings, such as climate (Sobel and Strecker, 2003), tectonics (Whipple and Tucker, 1999) and sea level changes (Van Wagoner et al., 1990). However, recent experimental and theoretical studies show that these autogenic processes can produce stratigraphic products that mimic sedimentary successions produced by allogenic forcings (Sheets et al., 2002; Kim and Paola, 2007; Straub et al., 2009; Hajek et al., 2010; Straub et al., 2015). This complicates our ability to invert stratigraphic records for paleo-environmental signals.

Another issue that limits our capacity to confidently extract environmental signals is signal degradation during sediment transport and deposition. A recent study by Jerolmack and Paola (2010) used numerical models to conduct experiments which show that autogenic processes can destroy environmental signals before they are transferred into the stratigraphic record. Specifically, they suggest that when the magnitude and time scale of environmental signals overlap those of a system's autogenic processes, they are prone to shredding. The Jerolmack and Paola (2010) theory provides a novel framework to construct null-hypothesis for the conditions necessary to propagate environmental signals across landscapes. However, conditions necessary to transfer a signal into the stratigraphic record remain unconstrained.

Furthermore, while the Jerolmack and Paola theory provides a general framework to describe signal propagation, work remains to define how to apply this theory for specific classes of environmental signals, such as changes in rock uplift rate or relative sea level.

A third challenge to the extraction of environmental signals from surface processes and stratigraphy is a lack of quantitative tools and metrics for signal analysis. The time and space scales of morphodynamic processes and products display a strong degree of stochasticity due to non-linear processes. As such, identification of signals in surface processes and their products requires a statistical approach. Unfortunately, the development of statistical metrics to describe these processes and products has lagged behind our development of deterministic theory. As such, the primary goals of this thesis are to (1) develop theory to define thresholds for the propagation and storage of specific environmental signals, such as changes in rock uplift rates and relative sea level, across the Earth's surface and into the stratigraphic record and (2) the development of metrics to quantify the magnitude and time scale of surface processes and products that are important for environmental signal propagation and storage.

To accomplish these goals, I utilize existing and newly developed metrics to quantify how deterministic and stochastic processes affect the propagation and storage of signals from sediment sources to sinks. Starting with erosional landscapes, I use a numerical model to explore how deterministic processes influence the conversion of rock uplift changes into sediment flux signals. Specifically, I examine how the

duration of rock uplift rate change affects time series of sediment flux exiting erosional landscapes. Next, I move my focus to deltaic depocenters to quantify how sediment properties, specifically sediment cohesion, influence the space and time scales of autogenic processes. Finally, I develop theory to define the conditions necessary for the storage of relative sea level signals in the stratigraphic record. I then use this theory to examine the stratigraphic storage of relative sea level cycles during icehouse and greenhouse Earth conditions.

With the advance of remote sensing technology, we have increased our capacity to observe some autogenic processes on the Earth's surface, such as river avulsions (Aslan and Blum, 1999; Buehler et al., 2011; Edmonds et al., 2016) and detect how landscapes respond to some environmental forcings (Syvitski et al., 2012). However, it is difficult to obtain the quantity of direct measurements necessary to characterize the natural variability in the time and space scales of autogenic processes and the response of transport systems to environmental forcings. As a result, many scientists attempt to use numerical modelling and physical experiments to explore how autogenic processes and allogenic forcings influence the evolution of landscapes (Whipple and Tucker, 1999; Heller et al., 2001; Tucker et al., 2001; Sheets et al., 2002; Whipple and Tucker, 2002; Edmonds and Slingerland, 2010; Kim et al., 2010; Armitage et al., 2011; Straub and Esposito, 2013; Caldwell and Edmonds, 2014). For example, Armitage et al. (2011) utilize a one dimensional numerical model to explore how erosional systems respond to step changes in precipitation rates and how the sediment flux signals delivered from erosional systems are recorded in adjacent

sedimentary basins. They find that there is a transient period of adjustment before the sediment flux reaches steady state and this delayed equilibrium sediment flux might lead to a characteristic stratigraphic pattern.

Although insights from these studies advance our understanding of the influence of autogenic and allogenic forcings on the evolution of landscapes, many questions remain unanswered. For instance, there is a possibility that changes in allogenic forcings might not always be recorded in the sediment flux signal at the outlet of an erosional landscape. If some signals make it to the outlet of an erosional catchment, while others do not, what properties of the allogenic forcing determine signal propagation? How do the properties of the upstream sediment flux, such as sediment cohesion, influence the architecture of stratigraphy over time scales important to the filling of sedimentary basins? Finally, how might the magnitude and time scale of autogenic processes influence the storage of environmental signals, such as relative sea level change? In order to answer these questions, I use a suite of previously and newly developed metrics in this thesis, with the aim of discriminating autogenic and allogenic products from sediment sources to sinks.

This thesis includes three major chapters and each chapter can stand on its own, although they are closely related. In the second chapter, I use the Channel-Hillslope Integrated Landscape Development (CHILD) (Tucker et al., 2001) model to explore how sediment flux from an erosional landscape responds to non-steady rock uplift. Many studies assume a sediment flux from erosional landscapes and focus on how sediment flux signals associated with tectonics propagate to depositional basins

(Jerolmack and Paola, 2010; Simpson and Castelltort, 2012). However, some tectonic signals likely do not translate into sediment flux signals at the outlet of erosional landscapes. In order to test this possibility, I conduct a series of numerical experiments with different temporal patterns of rock uplift rate. The modeled uplift rate in each experiment varies between a high and low value. Between experiments we vary the duration of the high and low uplift intervals, but not the magnitude of the uplift rates. Analyses of the sediment flux signals at the outlet of erosional landscapes show that there is a time lag between tectonic perturbations and the response to a perturbation as seen in time series of sediment flux. In order to link the duration of rock uplift changes with the sediment flux response, I quantify two lag times that respond to high and low rock uplift rate, respectively. Results from this chapter help place quantitative limits on the properties that an uplift signal must have to produce a faithful sediment flux signal at the outlet of an erosional watershed, and therefore quantifies what uplift signals could plausibly be stored in a downstream sedimentary system.

The upstream sediment flux supply might have significant variations due to changes in rock uplift rates in the erosional landscape, which can greatly influence the architecture of stratigraphy in a sedimentary basin. However, even if there is no variation in the magnitude of sediment supply, other properties of the sediment transport system, such as grain size, minerology and the type and density of vegetation, can influence the evolution of alluvial basins. In the second chapter, I use physical experiments to examine how sediment cohesion affects deltaic

morphodynamics and how these surface dynamics translate into stratigraphic architecture over basin filling time scales. Specifically, I examine data from three physical experimental stages that share the same forcing conditions, with the exception of the amount of a polymer added to a sediment mixture, which influences sediment cohesion in a manner similar to vegetation and/or dewatered clays (Hoyal and Sheets, 2009; Martin et al., 2009). First, I use Gust Erosion Microcosm System (GEMS) (Gust and Müller, 1997) experiments to quantify the influence of the polymer on the sediment cohesion. Next I use statistical metrics to characterize the temporal and spatial scales of important autogenic processes. Finally, I compare and characterize differences in the resulting stratigraphy of each experimental stage. Specifically, I characterize spatial depositional patterns and the segregation of fine from coarse sediment. The statistical characterization suggests that sediment cohesion reduces the mobility of the geomorphic system and that this results in an increase in the persistence of depositional trends and the segregation of fine from coarse sediment in deltaic stratigraphy. Results from this chapter further our understanding of one critical parameter that helps determine the pace of autogenic processes and how these processes set stratigraphic trends.

While the numerical modelling and physical experiments employed in chapters two and three isolate the influence of allogenic or autogenic processes, in field systems autogenic process are generally influenced by changing environmental forcings. Understanding how autogenics and allogenics interact is crucial for inverting stratigraphic successions for the paleo-environmental signals. I tackle a component of

this research question, the interaction of changing RSL with autogenic process, in chapter four. Deltaic systems are sensitive to large magnitude and long period RSL change, which influences stratigraphic architecture (Blum and Törnqvist, 2000). However, the range of amplitudes and periodicities of RSL cycles stored in stratigraphy remains unknown. Using estimates of the magnitude and time scale of autogenic processes contained in chapter three, I test the major hypothesis that RSL cycles with magnitudes and periodicities less than the spatial and temporal scales of the internal dynamics of deltas cannot confidently be extracted from the physical stratigraphic record. To understand the possible effect of stratigraphic signal shredding on Milankovic scale RSL cycles, I compile a database of channel depths and autogenic time scales for medium and large field scale deltaic depocenters. I also measure the basic architecture characteristics of stratigraphy in each RSL cycle experiment, including the fraction of each deposit composed of sand and channel body aspect ratios, to further test our major hypothesis. Results from this study set quantitative limits on the range of paleo-RSL information that can be extracted from stratigraphy, which could aid the prediction of deltaic response to climate change.

Chapter 2

Some signals are not as they appear: How do erosional landscapes transform tectonic history into sediment flux records?

ABSTRACT

A change in tectonics affects erosion rates across a mountain belt, leading to a period of non-steady sediment flux delivery downstream. The nonlinear relationship between tectonics and sediment flux at the outlet of an erosional catchment increases the difficulty in confidently extracting paleo-tectonic signals from sedimentary records. We use a numerical landscape evolution model to define quantitative thresholds on the duration of rock uplift intervals that are necessary for tectonic signals to be faithfully preserved in sediment flux records at the outlet of an erosional landscape. Specifically, we explore how the sediment flux responds to non-steady rock uplift, focusing on time lags and magnitudes of sediment flux records relative to durations of rock uplift. We observe that (1) the sediment flux does not always record changes in the rock uplift rate when the duration of a rock uplift interval is less than 25% of landscape response time, or time for a landscape to transition from one steady state to another after a perturbation; (2) a non-linear response between erosion rates and tectonic perturbations can result in increasing sediment flux through time even after rock uplift rate decreases; (3) rock uplift rates interpreted from the sediment flux at the outlet of a transient erosional watershed are not representative of the true rock

uplift rate values. These results illustrate conditions under which tectonic signals have the potential to be stored in the stratigraphic record and the degree to which signals may be lost in an erosional system.

2.1INTRODUCTION

The rock record has been interpreted as a window on past tectonic and climatic conditions (Hutton, 1788; Ahnert, 1970). However, before environmental forcings can be recorded in sedimentary deposits, sediment containing signals needs to be delivered from erosional landscapes. Studies (Simpson and Castelltort, 2012; Romans et al., 2015) often simplify the relationship between environmental forcing and sediment flux from the erosional landscape as a linear one in order to focus on how signals are transmitted through the bypass zone, or transport zone. These studies suggest that signals can be distorted or even destroyed through internal river dynamics (Jerolmack and Paola, 2010). However, the puzzle likely extends upstream of the bypass zone and patterns in sediment flux from erosional landscapes may be distinct from patterns in the forcing. How environmental signals are delivered from erosional landscapes to the bypass zone remains an open question (Allen, 2008; Armitage et al., 2011; Simpson and Castelltort, 2012; Armitage et al., 2013; Forzoni et al., 2014). Without an answer to this question, it is impossible to build a complete framework for signal propagation from source to sink.

Previous studies used 1D or spatially-lumped numerical models to explore the nonlinear responses between sediment flux and rock uplift changes (Armitage et al.,

2011; Forzoni et al., 2014). These studies focus on how sediment flux responds to both a single change in rock uplift rate and/or periodic changes. Both found that the sediment flux responds immediately to initial rock uplift changes, but that there is a transient period of adjustment before the sediment flux reaches steady state. They suggested this delayed steady-state sediment flux leads to a characteristic stratigraphic pattern. However, neither study recognized the possibility that rock uplift signals may not be recorded in the sediment flux. In addition, neither attempted to set a quantitative threshold for the duration of rock uplift that allows the sediment flux to faithfully capture rock uplift changes.

In this study, we explore whether there is a relationship between patterns in the sediment flux delivered from an erosional landscape and the rock uplift history. More specifically, we ask: (1) Under what conditions are changes in rock uplift rate simultaneously recorded in the sediment flux delivered from an erosional landscape? and (2) How is the magnitude of the sediment flux related to the magnitude of the rock uplift rate in a transient erosional landscape? To address these questions, we force a numerical landscape evolution model with different temporal patterns of rock uplift rate. We attempt to simplify as many aspects of the study as possible. For example, rock uplift rate varies as a step function and fluvial incision is controlled by the simplest available process model, stream power (Whipple and Tucker, 1999). This study places quantitative limits on the properties that an uplift signal must have to produce a faithful sediment flux signal at the outlet of an erosional watershed, and therefore quantifies what uplift signals could plausibly be stored in a downstream

depositional basin.

2.2 DESCRIPTION OF NUMERICAL MODEL AND EXPERIMENTS

We use the CHILD landscape evolution model (Tucker et al., 2001) to examine the sediment flux response from a synthetic erosional watershed to different rock uplift patterns. We model fluvial incision using the detachment-limited stream-power model (e.g., Whipple and Tucker, 1999), which simulates bedrock incision as a power-law function of drainage area and slope (Table 2.1) and does not allow for deposition of sediment. Sediment flux at the watershed outlet is calculated as the summation across the model domain of the product of local incision rate and local cell area (see Figure 2.1A for the geometry of the model domain). We use a pulsed pattern of rock uplift in which the rate alternates between a low and high value, 1 mm/yr and 10 mm/yr, respectively. The uplift period (T) is defined as the sum of the duration of one high (t_H) and one low (t_L) interval of uplift (Figure 2.1B), and the ratio of t_H to T is used to calculate the percentage of the period during which the rock uplift rate is high (P_H), and similarly, the low uplift percentage P_L is equal to 100-P_H.

The initial condition for all numerical experiments is a steady-state landscape with a rock uplift rate of 1 mm/yr. We perturb the initial steady state with the pulsed rock uplift pattern and vary P_H and T among the experiments. P_H and T are chosen based on the response time (RT), the time determined from model experiments for the landscape to transition from one steady state to another following a rock uplift rate change (See Appendix to chapter 2, table S2.1). All model experiments are run for ten

million years, allowing for at least five uplift periods. For each of the three T values, we perform four experiments with different P_H values (table S2.1). Based on observations of these experiments, we conduct an additional experiment, where T is 200% of RT and P_H = 50%. Natural rock uplift histories are more complex than the repetitive, simple uplift patterns that we model (Meigs et al., 2008). However, we specifically use a simple experimental set-up in order to maximize the potential for preserving a link between tectonic history and signals in the sediment flux history.

2.3 RESULTS

We first examine the time series of sediment flux at the watershed outlet in each experiment (Figs. 2.1B & 2.2). The general pattern of sediment flux in each experiment follows a similar cycle. The sediment flux increases immediately when the rock uplift rate increases in the initial steady-state landscape. When the rock uplift rate decreases for the first time, the sediment flux does not decrease immediately except in the experiments where t_H is equal to or greater than the response time (Figure 2.2D & Figure S2.4). After an initial adjustment period, the duration of which varies depending on T and P_H, the sediment flux reaches a dynamic equilibrium with the tectonic forcing. At this point in all of the experiments, the period of the sediment flux signal is the same as that of tectonic forcing (T). However, the details of the sediment flux record, such as the time necessary for the sediment flux to respond to any given rock uplift change, and the magnitudes of the maximum and minimum sediment flux, vary with T and P_H.

To quantify the influence of T and P_H on the time until the sediment flux responds to the rock uplift change, we define and measure two variables: (1) the lag time for responding to an increase in rock uplift rate (LT_H) during dynamic equilibrium, which is the time between the beginning of the high uplift rate interval and the beginning of an increase in the sediment flux; and, similarly, (2) the lag time for responding to a decrease in rock uplift rate (LT_L) during the dynamic equilibrium (Figure 2.1B). In all experiments, there is no lag time (LT_H is equal to zero) initially, because the initial landscape is in steady state.

Once dynamic equilibrium is reached, there is a time lag for the sediment flux to respond to rock uplift changes (both high and low), with the exception of the experiments in which the landscape reaches steady state before the rock uplift changes. We measure all time lags following a change in rock uplift rate and calculate the mean LT_H and LT_L for each experiment. In experiments with the same T value, the mean LT_H value decreases as t_L increases (Figure 2.3A). An increase in the duration of the previous low rock uplift rate interval allows the landscape to be closer to a low-uplift rate steady state when the uplift rate increases. Similarly, the mean LT_L value also decreases as t_H increases (Figure S2.2A). In all experiments, LT_L and LT_H are always smaller than t_L and t_H, respectively. For the experiments where T is 25% of RT, LT_H approaches zero even though the duration of low uplift rate is far from the response time. This is because LT_H is limited by the small value of t_H (Figs. 2.3A & B, smallest value of LT_H for T=25%RT experiment). The ratio of LT_H to t_H, or similarly LT_L to t_L, indicates the degree to which the system is out of phase. For example, if LT_H

= 0.5 t_H, then for half of the high rock uplift period, the sediment flux is continually decreasing. There are cases in which the sediment flux is decreasing (increasing) for more than half of the high (low) rock uplift period (Figure 2.3B and Figure S2.2B).

We also quantify the minimum and maximum observed sediment flux relative to the equilibrium minimum and maximum sediment flux ($Q_s^{\min}/Q_{s\_eq}^{\min}$ and $Q_s^{\max}/Q_{s\_eq}^{\max}$, respectively). Comparing among the experiments with the same T, $Q_s^{\max}/Q_{s\_eq}^{\max}$ increases as the duration of high rock uplift rate increases (left to right in the panels in Figure 2.2; Figure 2.4A). This ratio also varies as a function of t_L (t_L=T-t_H), as illustrated by experiments with similar t_H but with different T (e.g., experiments within oval shape in Figure 2.4A). A shorter duration of low uplift means that $Q_s^{\min}$ is further from $Q_{s\_eq}^{\min}$. As such, a similar value of t_H and a smaller value of t_L leads to higher values of $Q_s^{\max}$ and $Q_s^{\max}/Q_{s\_eq}^{\max}$. Barring the two experiments in which t_H is equal to or greater than the response time, $Q_s^{\max}/Q_{s\_eq}^{\max}$ never reaches one. We observe similar trends for $Q_s^{\min}/Q_{s\_eq}^{\min}$, except that $Q_s^{\min}/Q_{s\_eq}^{\min}$ decreases to unity as t_L increases to RT (Figure S2.3)

These systematic changes in $Q_s^{\min}$ and $Q_s^{\max}$ lead to a pattern in their difference, here referred to as ΔQ_s. For a given T, as P_H increases from 25% to 50%, ΔQ_s increases; as P_H increases from 50% to 90%, ΔQ_s decreases (Fig S2.1). However, for a given P_H, ΔQ_s increases as T increases. These trends in ΔQ_s are observed despite the fact that the difference between the high and low rock uplift rates does not vary among the experiments.

In order to quantify how the uplift signals are preserved in the sediment flux records, we normalize ΔQ_s by the difference between maximum and minimum equilibrium sediment flux, or $(Q_s^{\max} - Q_s^{\min})/(Q_{s\_eq}^{\max} - Q_{s\_eq}^{\min})$. If this normalized value were 1, it would mean that the difference in observed sediment flux perfectly characterizes the expected difference based on the rock uplift rates. Otherwise, it would mean that some information about tectonic signals is lost in these sediment flux signals. Our results show that this ratio increases with increasing T (Fig 4B, for a given t_H), which suggests $Q_s^{\min}$ and/or $Q_s^{\max}$ will be closer to $Q_{s\_eq}^{\min}$ and/or $Q_{s\_eq}^{\max}$, respectively. As a result, the implied uplift rates ($\frac{Q_s^{\min}}{A}$ and/or $\frac{Q_s^{\max}}{A}$) are closer to the real low and high uplift rate, respectively.

Even with the simple rock uplift patterns used here, some signals are not transmitted through the erosional system. In the experiments with the shortest periodicity (T= 25% RT) (Figure S2.1 A-D), the sediment flux continuously increases even while the rock uplift rate is low during the entire first two periods. This indicates that the sediment flux might not record any information about some short-duration rock uplift changes. It takes time for rock uplift changes to propagate upstream (Figure 1A). As a result, the downstream part of the landscape can erode at a low rate due to a decrease in rock uplift rate, but if this signal has not reached a large enough part of the landscape, it may not be evident in the sediment flux.

2.5 DISCUSSION

In this study we are primary interested in (1) the lag time between rock uplift rate changes and sediment flux responses that results from the propagation of erosion signals (knickpoints) throughout a drainage network and (2) necessary conditions for an uplift signal to be evident in the sediment flux record at the outlet of an erosional watershed. Although previous studies have shown that the peak erosion rate can lag behind uplift changes (Willenbring et al., 2013), the influence of lag time on the details of the sediment flux history remains unknown. We find that when the rock uplift rate oscillates between low and high rates, the lag time decreases as the duration of the pervious uplift interval increases. If the uplift rate interval is longer than the response time, there will be no time lag between the sediment flux response and the rock uplift rate change. Our results suggest that the lag time is strongly influenced by the relationship between duration of tectonic events and landscape response time, which can vary greatly (Whipple, 2001).

In order to predict when there will be a lag time in the sediment flux response to a change in uplift rate, we define the ratio of the uplift duration (t_U) to the response time (RT, calculated using equation 6 with n=1 in Whipple, 2001) as the non-dimensional time (T_{ND}):

$$T_{ND} = \frac{t_U}{RT} = \frac{t_U}{\mathrm{k}_a^{-m/n}\left(1 - \frac{\mathrm{hm}}{\mathrm{n}}\right)^{-1}\left[\left(\frac{A}{k_a}\right)^{\frac{1}{h}\left(1-\frac{hm}{n}\right)} - x_c^{(1-hm/n)}\right] \Big/ K} \quad (1)$$

where k_a and h describes the relationship between channel length and drainage area (Hack, 1957); K is the erodibility coefficient in the stream power model (SPM) which

decreases with increasing rock strength and with less erosive climate conditions; x_c is distance from drainage divide to channel head; and m, and n are the exponents on drainage area and slope, respectively, in the SPM. The response time is most sensitive to the erodibility coefficient, but also varies with drainage area (Figure 2.3C). The exponent on drainage area in equation 1, $\frac{1}{h}\left(1-\frac{hm}{n}\right)$, is about 0.1 for a typical h value of 1.67 and m=0.5 and n=1. As a result, response time is not very sensitive to drainage area (Whipple and Tucker, 1999). Our modeling results suggest that there is a lag time when T_{ND} is smaller than 1, and that the previous uplift duration is the important value to consider (Figure 2.3A). Based on equation 1, T_{ND} is likely to be less than 1 in larger watersheds with harder to erode rocks or less erosive climates, that is, with smaller K values.

As a result of the lag time, the sediment flux can be out of phase with uplift rate changes. We illustrate a number of cases in which the sediment flux is decreasing for at least half of the time that the uplift rate is high (Figure 2.3B). Although these are not completely out of phase, these examples illustrate that great caution should be taken when assuming that increasing (decreasing) sediment flux indicates that a landscape is responding most recently to an increase (decrease) in rock uplift rate. The landscape morphology (Kirby and Whipple, 2012), in conjunction with the sediment flux, can help one to accurately judge whether uplift rate has most recently increased or decreased. However, information on landscape morphology is not usually available for past landscapes that produced the sediment flux stored in a sedimentary basin.

Similarly to previous studies (Armitage et al., 2011; Forzoni et al., 2014), our results also indicate that using sediment flux to reconstruct the magnitude of historical rock uplift rates can be incorrect without fully considering the nonlinear response of sediment flux to uplift changes and the transient conditions of a landscape. In our study, the ratio between high and low rock uplift rate is constant, whereas the difference between the maximum and minimum sediment flux rate can vary with the duration of high and low rock uplift rate, which control the lag time (Figure 2.4B; Figure S2.3B). In other words, the duration of high and low rock uplift control how far a landscape is from steady state, which controls how the sediment flux responds to further perturbations.

When the rock uplift intervals are shorter than the response time, the implied rock uplift rate, as calculated from sediment flux, deviates from the actual rock uplift rate. Following this, we explore how the normalized sediment flux, $(Q_s^{\max} - Q_s^{\min})/(Q_{s\_eq}^{\max} - Q_{s\_eq}^{\min})$, or ΔQ_s, captures the difference in rock uplift changes, because ΔQ_s is what will potentially be preserved in a deposit. Our results suggest that the sediment flux signal has the largest potential to illustrate the magnitude of rock uplift changes if the duration of high and low uplift rates are both at least equal to or greater than response time (Figure 2.4B). With information on the duration of uplift rates and landscape response time, these quantitative thresholds illustrate a condition when we can faithfully interpret past rock uplift rates from the sediment flux. This could be applied in relatively well-constrained basin-and-range settings, in which sediment is deposited directly in an alluvial fan at the mouth of the watershed,

the depositional events are dateable, and the upstream drainage area can be accurately estimated.

Previous studies highlight that autogenic (internal) processes play an important role in dampening or destroying environmental signals (Jerolmack and Paola, 2010; Van De Wiel and Coulthard, 2010). Even without autogenic processes in our modeling, we find that relatively short duration changes in rock uplift rate may not translate to a signal in the sediment flux. The most likely interpretation of a sedimentary deposit in which the sediment flux steadily increased with time would not be that upstream rock uplift rates increased and decreased through time. However, our results suggest that this is a possibility (Fig S2.1A-D). More studies are needed to fully quantify what tectonic signals get lost in the sediment flux, and therefore have no chance of being preserved in stratigraphy.

Under the simplest of circumstances, we place a quantitative threshold on the duration that periods of rock uplift must have to be clearly stored in the sediment flux record at the outlet of erosional landscape. Lag times and dampening of the sediment flux signal with respect to what would be expected under steady-state conditions might complicate our ability to reconstruct tectonic histories. However, knowledge of the controls on lag time and ΔQ_s will help overcome some of these complications, thus reducing error in our interpretation of tectonic signals from the ancient rock record. Further study could potentially incorporate autogenic processes, such as landslides and river capture, to examine their influence on lag time and the preservation potential for tectonic signals.

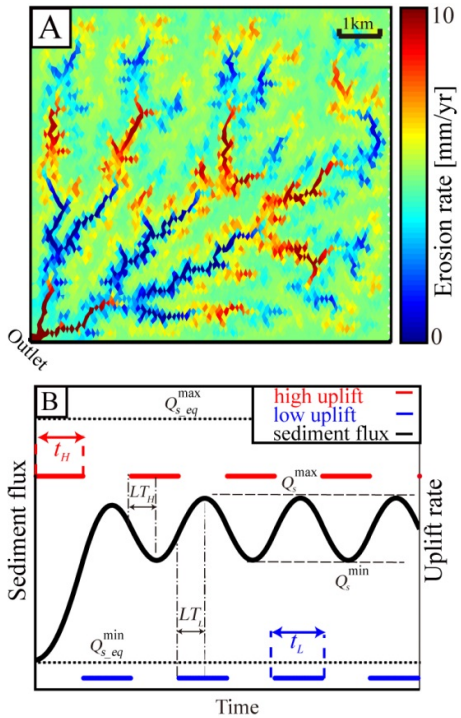

Figure 2.1 Maps and data from the model scenario with T = 75% of RT and PH equal to 50%. Maps and data from the model scenario with T = 75% of RT and P_H equal to 50%. (A) Erosion rate map of modeled landscape at 0.3 million years after the start of the perturbation of rock uplift rate. (B) Schematic sediment flux time series. The dashed lines illustrate the maximum (Q_s^{max}) and minimum (Q_s^{min}) modeled sediment flux after the sediment flux reaches dynamic equilibrium. The dotted lines show the equilibrium sediment fluxes, $Q_{s\_eq}^{max}$ and $Q_{s\_eq}^{min}$, which are calculated as the product of drainage area of the erosional landscape and the high or low rock uplift rate, respectively. The dash-dot lines exhibit the LT_L and LT_H

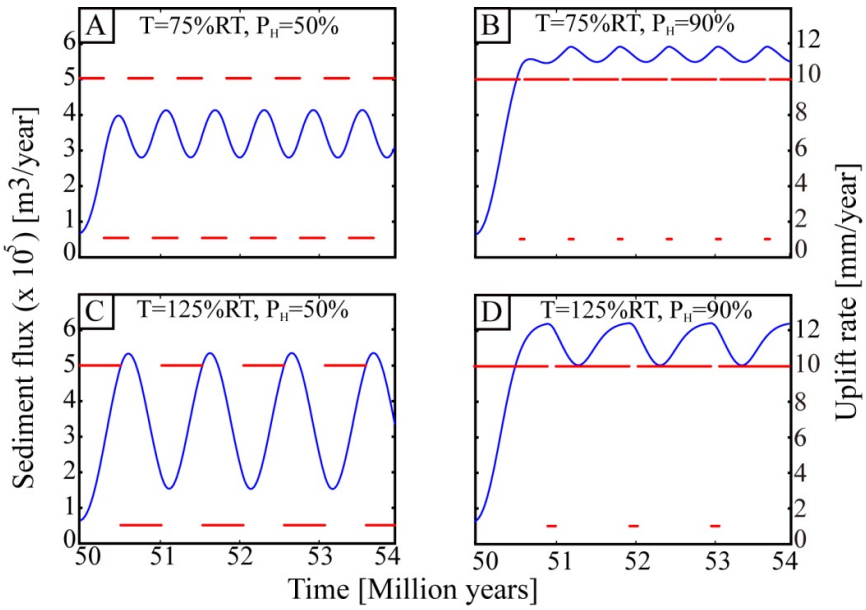

Figure 2.1 Time series of sediment flux for the uplift perturbation experiments. Time series of sediment flux for the uplift perturbation experiments. **(A-D)** The red lines represent the time series of uplift and the blue line shows how sediment flux responds to the change in uplift rate.

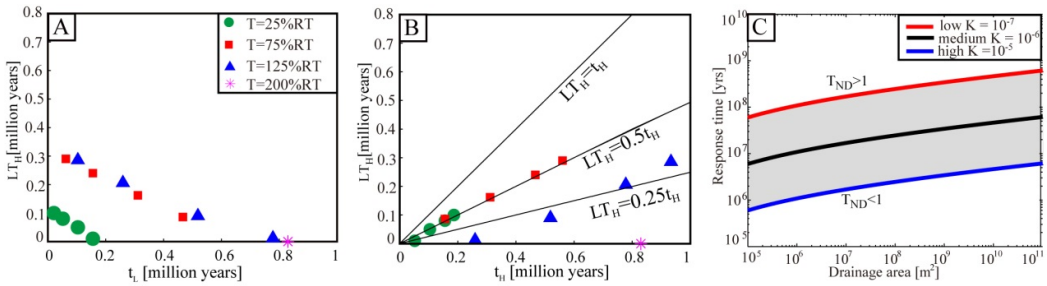

Figure 2.2 Variation in lag time and response time (A) LT_H as a function of the duration of low rock uplift; (B) LT_H as a function of the duration of high rock uplift. The black lines illustrate where LT_H is equal to 25%, 50% and 100% of the duration of high rock uplift rate. (C) Response time changes with drainage area and erodibility coefficient. The blue, black and red lines illustrate the response time as a function of drainage area for different erodibility values. The gray region shows the possible values of response time for different systems given this relatively wide range of erodibility values. Unless the time scale of tectonic perturbation is greater than the response time, or above the appropriate line, then $T_{ND} > 1$, we predict that there will be a lag time in the sediment flux response.

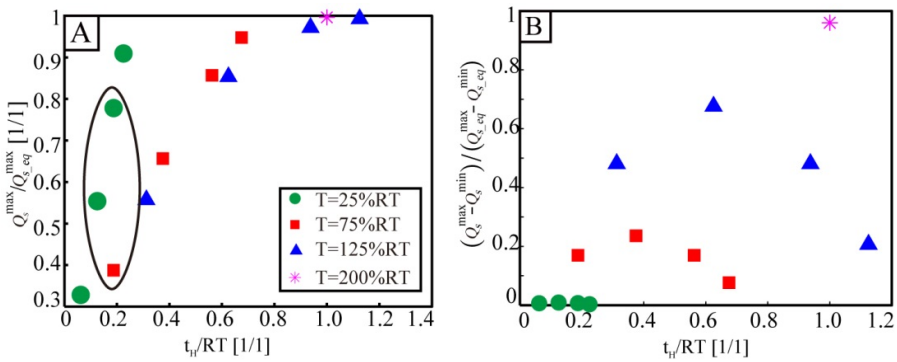

Figure 2.3 (A) $Q_s^{\max}/Q_{s\_eq}^{\max}$ as a function of t_H/RT. The experiments within the oval have similar t_H/RT ratio (B) Normalized sediment flux, $(Q_s^{\max}-Q_s^{\min})/(Q_{s\_eq}^{\max}-Q_{s\_eq}^{\min})$, as the function of t_H/RT.

Domain size	Resolution (m)	*m*	*n*	*K* (yr^{-1})
8 km x 8 km	100	0.5	1	0.00001

Table 1 Experimental parameters used in all CHILD numerical experiments. The stream power model is described by the equation: $E = KA^{m}S^{n}$, where K is a dimensional erosional efficiency factor affected by climate and the type of bedrock (yr^{-1}), Q is fluvial discharge (m^3/yr), S is the slope (m/m), m and n are positive dimensionless constants and depend on hydrology, hydraulic geometry, and erosion process

Appendix to Chapter 2

A2.1 LT_L

In the experiments with constant T, mean LT_L decreases with an increase in t_H, the duration of previous high rock uplift rate (Figure S2.2A). An increase in the duration of previous high rock uplift rate allows the landscape to be closer to steady state when the uplift rate decreases. In addition, LT_L can have a value greater than 50% of t_L (Figure S2.3B), which means sediment flux is out of phase (sediment flux continuously increasing while rock uplift rate is low)with rock uplift changes for at least half duration of rock uplift changes.

A2.2 $Q_s^{\min}/Q_{s\_eq}^{\min}$

Comparing among the experiments with the same T, $Q_s^{\min}/Q_{s\_eq}^{\min}$ decreases as the duration of low rock uplift rate increases (Figure S2.3A). Our results show that $(Q_s^{\max}-Q_s^{\min})/(Q_{s\_eq}^{\max}-Q_{s\_eq}^{\min})$ increases with increasing T (Fig 4B), which suggests that $Q_s^{\min}$ and/or $Q_s^{\max}$ will be closer to $Q_{s\_eq}^{\min}$ and $Q_{s\_eq}^{\max}$, respectively. As a result, the implied uplift rates ($\frac{Q_s^{\min}}{A}$ and/or $\frac{Q_s^{\max}}{A}$) might be more close to the real low and high uplift rate, respectively. For a given T, the largest ratio occurs when high and low uplift rate has the same duration.

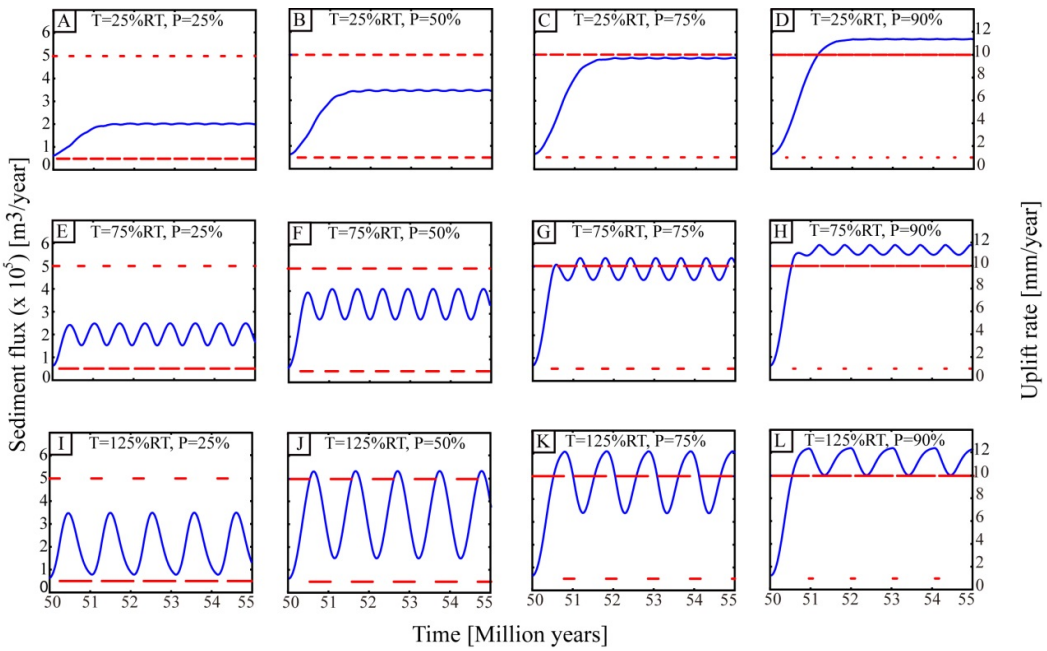

Figure S2.1 Time series of sediment flux**.** (A-L) The red lines represent the time series of uplift and the blue line shows how sediment flux responds to the change in uplift rates.

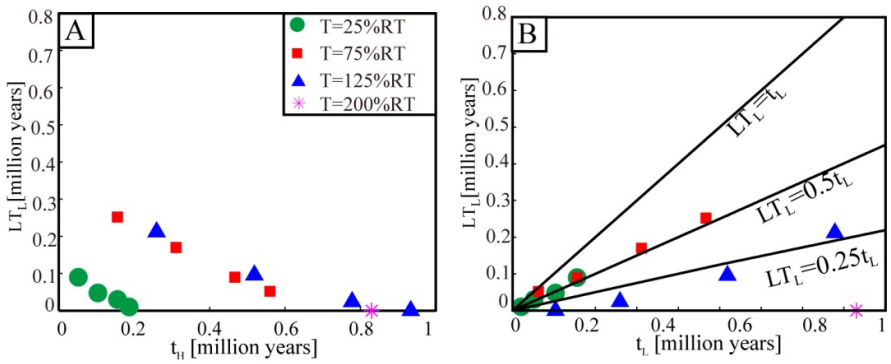

Figure S2.2 Variation in lag time. (A) LT_L as a function of the duration of high rock uplift; (B) LT_L as a function of the duration of high rock uplift. The black lines illustrate the cases in which LT_L is equal to 25%, 50% and 100% of the duration of low rock uplift rate.

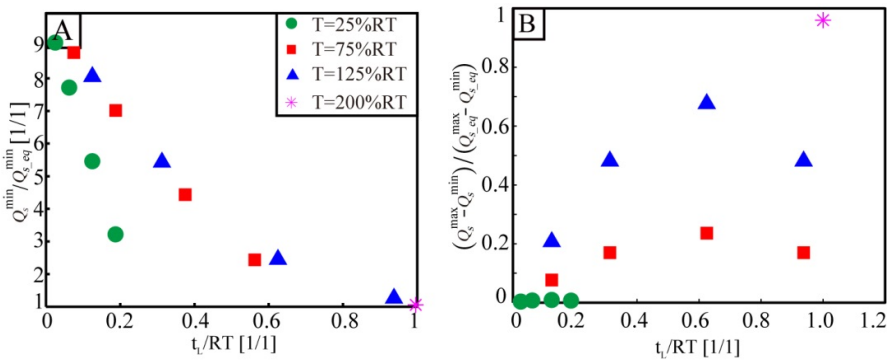

Figure S2.3 (A) $Q_s^{min}/Q_{s\_eq}^{min}$ as the function of t_L/RT. (B) Normalized sediment flux, $(Q_s^{max}-Q_s^{min})/(Q_{s\_eq}^{max}-Q_{s\_eq}^{min})$, as a function of t_H/RT.

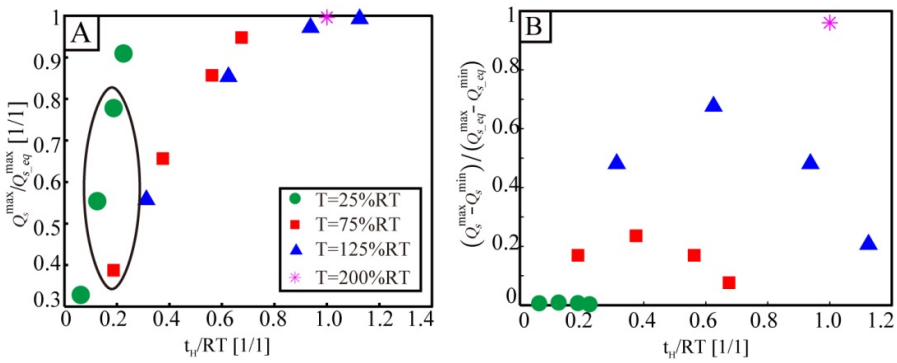

Figure S2.4 Time series of sediment flux where T is 200% of RT and P_H is 50%.

Experiments	T (Ma)	P_H (%)	t_H (Ma)	t_L (Ma)
T=25%RT, P=25%	0.32	25	0.08	0.24
T=25%RT, P=50%	0.32	50	0.16	0.16
T=25%RT, P=75%	0.32	75	0.24	0.08
T=25%RT, P=90%	0.32	90	0.28	0.04
T=75%RT, P=25%	0.95	25	0.24	0.71
T=75%RT, P=50%	0.95	50	0.475	0.475
T=75%RT, P=75%	0.95	75	0.71	0.24
T=75%RT, P=90%	0.95	90	0.85	0.1
T=125%RT, P=25%	1.58	25	0.40	1.18
T=125%RT, P=50%	1.58	50	0.79	0.79
T=125%RT, P=75%	1.58	75	1.18	0.40
T=125%RT, P=90%	1.58	90	1.42	0.16

Table S2.1 The periodicity and proportion of high rock uplift among experiments. In a preliminary experiment, we perturb the steady-state landscape with a constant high rock uplift rate, 10 mm/yr, in order to estimate the response time (RT) for the landscape to be 1.26 Ma. Note that although we do not use the relationship presented in equation 1 for calculating response time, we find that our results scale with this equation.

Chapter 3

Influence of sediment cohesion on deltaic morphodynamics and stratigraphy over the basin-filling time scale

ABSTRACT

Results from physical and numerical experiments suggest that sediment cohesion influences deltaic morphodynamics by promoting the development and maintenance of channels. As a result, cohesion is thought to increase the magnitude and time scales of internally generated (autogenic) processes and their stratigraphic products. We test these hypotheses by examining the surface processes and stratigraphic products from a suite of physical experiments where the influence of cohesion is isolated over basin filling time and space scales. Given the stochastic nature of autogenics at these scales, we develop and employ a range of statistical tools and metrics. We observe that 1) an increase in sediment cohesion decreases lateral channel mobility and thus increases the time necessary to regrade deltaic surfaces; 2) enhanced channelization, due to sediment cohesion, increases the time necessary for the deposits of autogenic processes to average together and produce stratigraphic products with shapes set by the generation of regional accommodation; 3) cohesion promotes pumping of suspended sediment to terrestrial overbank and marine environments, which decreases the volume of channel, relative to overbank and marine deposits in the stratigraphic record. This increase in overbank and marine deposition changes the spatial distribution of sand in the stratigraphy, with higher cohesion linked to enhanced

segregation of fine materials from coarse sand in the experimental deposits. Combined, these results illustrate how the stickiness of sediment is fundamental in setting autogenic space and time scales and needs to be considered when inverting stratigraphic architecture for paleo-environmental history.

3.1 INTRODUCTION

Deltaic morphology is set by a plethora of forcings originating from both terrestrial and marine environments. Of these the most frequently discussed are the flux of sediment to the shoreline and the wave and tide climates summarized in Galloway's (1975) ternary diagram. However, over the last decade particular attention has been placed on the properties of sediment delivered to the coast. During this time field (Gibling, 2006; Davies and Gibling, 2010; Burpee et al., 2015), numerical (Edmonds and Slingerland, 2010; Caldwell and Edmonds, 2014), and laboratory (Peakall et al., 2007; Hoyal and Sheets, 2009; Martin et al., 2009; Tal and Paola, 2010; Straub et al., 2015) studies highlighted the importance of sediment cohesion to the morphology and stratigraphy of rivers and deltas. These studies emphasize that sediment cohesion is as important as the volumetric sediment flux, wave, and/or tide climate to the evolution of river deltas over lobe building time scales.

While studies conducted over the last decade expanded our appreciation of the implications of sticky sediment to deltaic morphodynamics, sediment properties, including cohesion, have long been discussed. For example, Kolb (1963) in a study of the Mississippi River Delta noted an increase in Pleistocene clays when approaching

the shoreline. He hypothesized that these cohesive sediments promoted the development of narrow and deep channels with slow migration rates. Studies by Orton and Reading (1993) and Tornqvist (1993) also noted the influence of fine grained and cohesive sediments on channel migration rates and the geometry of deltaic channels in both cross-section and planform.

It is now generally agreed upon that bank strength increases with cohesion, which decreases channel mobility and aids development of deltas with rugose shorelines. However, few studies have explored the implications of sediment cohesion on surface processes and stratigraphy over the space and time scales important for filling alluvial basins. The primary aim of this study is to fill this gap.

Many factors influence sediment cohesion, including the diameter, mineralogy, and compaction history of sediment, and the density and type of riparian vegetation (Davies and Gibling, 2011; Grabowski et al., 2011). Focusing first on sediment grain size, a suite of recent numerical experiments explored the influence of cohesion on deltaic morphodynamics by employing algorithms which link the critical shear stress for initiation of sediment motion, τ_{cr}, to sediment properties, including cohesion (Edmonds and Slingerland, 2010; Caldwell and Edmonds, 2014; Burpee et al., 2015). In many of these models particles finer than silt are assumed to be somewhat cohesive, so the finer the median particle size of the bed, the more cohesion is assumed. These studies observe that decreasing grain size (with associated increases in sediment cohesion) fundamentally changes the shape and depositional patterns of river deltas over lobe building time scales. For example, Edmonds and Slingerland (2010) and

Caldwell and Edmonds (2014) observe that deltas built from highly cohesive sediment form 'bird's-foot' morphologies with rugose shorelines, whereas systems characterized by less cohesive sediment result in fan-like deltas with smooth shorelines.

Riparian vegetation can also impart a strong control on the morphodynamics of deltas, partially due to its influence on sediment cohesion (Hicks et al., 2002; Murray and Paola, 2003; Rosen and Xu, 2013; Nardin and Edmonds, 2014). For instance, Murray and Paola (2003) use a cellular model to explore the influence of roots on channel patterns. This model suggest that roots aid river bank stabilization which can convert an otherwise braided system to a single thread channel, which has also been observed in physical experiments (Tal and Paola, 2007; Braudrick et al., 2009) . The influence of vegetation on paleo-channel morphodynamics can also be inferred from stratigraphy. In a suite of papers, Davies and Gibling (2010&2011) documented the evolution of channel patterns through geological time in response to the evolution of land plants. They show that stratigraphy of channelized sections dated to pre-Devonian times, and thus prior to land plants, has few single thread channel bodies.

While the work highlighted above demonstrates the importance of sediment cohesion, we still lack a clear picture as to how this influences deltaic stratigraphy over the time and space scales important for alluvial basin filling. For example, how do cohesive channel deposits stack together and how do they differ from the stacking of non-cohesive deposits? Does the introduction of cohesive sediment fundamentally

change the partitioning of sediment between channels and their overbanks, and if so how might this influence the segregation of fine from coarse sediment in their deposits? These questions are intertwined with the time and space scales of internal (autogenic) processes in deltaic morphodynamics including river avulsion, lobe switching and other processes that result in sediment storage and release (Beerbower, 1964; Paola, In Press).

Straub et al. (2015) took a few initial steps in the exploration of the influence of cohesion on morphodynamics and stratigraphic architecture over basin filling time scales. They conducted a set of physical experiments where the influence of sediment cohesion was isolated. In each experiment a self-organized delta was constructed through the introduction of water and sediment into an experimental basin that had a constant background base-level rise which promoted the development of tens of channel depths worth of stratigraphy. The constant forcing in each experiment allowed autogenic time and space scales to be isolated and explored. Their study focused on the influence of cohesion in setting autogenic shoreline dynamics and on deltaic sediment retention rates. They found that enhanced channelization resulting from sediment cohesion reduces sediment retention rates and increases the autogenic scales of shoreline transgressions and regressions.

In this study, we use the same set of physical experiments as Straub et al. (2015) but further the scope of exploration. Here the focus is on the stratigraphic implications of changes to deltaic morphodynamics induced by sediment cohesion. Given the stochastic nature of many autogenic surface processes and their stratigraphic products

(Paola, In Press), we take a statistical approach. This includes the use of previously developed metrics and the development of new metrics. We start by confirming in our experiments that an increase in sediment cohesion promotes the development of deep and narrow channels that are less laterally mobile. We then test two main hypotheses that relate surface processes to stratigraphic products. First, we hypothesize that the decrease in the mobility of sediment transport systems translates into increased persistence of depositional trends and an associated increase in the variability of these trends relative to the pattern of accommodation creation. Second, we hypothesize that the development of deeper channels with lower migration rates enhances the segregation of fine from coarse sediments in the resulting stratigraphy by reducing the reworking of overbank deposits by channels and promoting the pumping of fine sediments to overbank settings.

3.2 METHODS

3.2.1 Physical experiments

To examine the influence of sediment cohesion on deltaic surface dynamics and the resulting stratigraphy over time and space scales important to alluvial basin filling, we analyze data from three stages of two experiments (Figure 3.1). In recent decades, experiments have been used to explore how autogenic and allogenic processes influence stratigraphy at reduced scale (Muto and Steel, 2004; Kim et al., 2010; Straub and Wang, 2013). As outlined in a review by Paola et al. (2009), reduced-scale physical experiments produce spatial structure and kinematics that, although imperfect, compare well with natural systems despite differences in spatial and

temporal scales, material properties, and number of active processes.

The three experimental stages were conducted in the Tulane University Delta Basin, which is 2.8 m wide by 4.2 m long and 0.65 m deep (Figure 3.1). The three stages share identical forcing conditions with the exception of the cohesion of sediment entering the basin. Accommodation is created at a constant rate in all experiments by increasing ocean level utilizing a motorized weir that is in hydraulic communication with the basin. The computer controlled ocean level rise rate (r = 0.25 mm/hr) and input water (Q_w = 1.72 x 10^{-4} m^3/s) and sediment discharge (Q_s = 3.91 x 10^{-4} kg/s) allowed the shoreline to be maintained at an approximately constant location through the course of the experiments, but with super-imposed fluctuations associated with autogenic processes. The input sediment mixture was designed to mimic earlier experimental work (Hoyal and Sheets, 2009) and had a broad particle size distribution, ranging from 1 – 1000 μm with a mean of 67 μm and was dominantly quartz that was white in color. One quarter of the coarsest 23.5% of the distribution was commercially dyed to aid visualization of stratigraphic architecture. The sole difference in forcing conditions between the three experimental stages was the quantity of a polymer added to the input sediment. The enhanced cohesion provided by the polymer (New Drill Plus distributed by Baker Hughes Inc.) acts as a general proxy for the effect of vegetation and dewatered clays which enables the formation of deltas with strong channelization at sub-critical Froude numbers. As discussed by Hoyal and Sheets (2009), a volumetrically small amount of this polymer in dry granular form, when combined with water, coats a fraction of the sediment

grains with a viscous and cohesive film.

The three stages were performed over the course of two experiments. The first experiment began with the progradation of a delta into a shallow ocean with constant ocean level for 75 hours. This was followed by 300 hours of run-time and aggradation promoted through accommodation generation from base level rise. Input sediment during this stage had no added polymer and as such was only weakly cohesive due to electrostatic forces. We refer to this as the weakly cohesive stage. A second stage was run for 700 hours directly on top of the first stage. This stage included 40 g of dry granular polymer per 54 kg of sediment and had the same base level rise rate as the weakly cohesive stage. We refer to this as the moderately cohesive stage. The change in sediment cohesion at the start of the second stage resulted in the incision of channels into the weakly cohesive deposit. To isolate the characteristics of the moderately cohesive stage we focus our analysis on the final 500 hours of this stage. A strongly cohesive stage was conducted as part of a second experiment. This experiment also began with the progradation of a delta into an ocean of fixed depth, followed by aggradation driven by base-level rise. Unfortunately, input Q_s during this initial aggradation was below our target rate. Following a brief pause in base-level rise and adjustment of Q_s, the main phase of this experiment began. This stage ran for 900 hours with the same Q_w, Q_s, and ocean level rise rate as the first experiment, but with 80 g of polymer added per 54 kg of sediment. As such we refer to this as the strongly cohesive stage. While slight differences in initial ocean level, and initial delta size exist between stages, the duration of each stage was sufficient to

generate tens of channel depths worth of stratigraphy, thus reducing the importance of initial conditions on the bulk trends discussed below.

Topography was monitored with a 3D laser scanner, resulting in digital elevation models (DEMs) with a 5 mm horizontal grid in the down and cross basin directions, respectively and < 1 mm of vertical resolution for terrestrial regions and areas with water depths < 50 mm. One scan was taken near the end of each run hour with the flow on and dyed for visualization. These DEMs are co-registered with digital images collected by the scanner which allows the flow field to be directly tied to topography. A second scan was collected at the end of each run hour with the flow off for the highest possible resolution. Due to data outages in regions of deep water in distal basin locations, we limit our analysis to a region defined by a radius of 1.3 m from the basin entrance. This region was generally either delta top or upper delta foreset over the course of each experiment. This temporal and spatial resolution was sufficient to capture the meso-scale morphodynamics of the delta-top systems (e.g. channel and lobe avulsions). We also collected digital images of the active delta top with a Cannon G10 camera every 15 minutes with input water dyed to further aid morphodynamic analysis.

Finally, at the end of each experiment we sectioned the deltas along cross-sectional transects at 0.89 m and 1.3 m from the basin infeed point (Figure 3.1B). This was done by inserting a metal wedge into the deposit after the water level in the basin was raised to an elevation which flooded the entire deposit. The metal wedge was then filled with dry ice and methanol which resulted in a chemical reaction

that lowered the temperature of the wedge to a value sufficient to freeze the pore water in the deposit and the surrounding deposit to the wedge. The wedge was then extracted from the basin providing a view of the preserved stratigraphy which was then photographed with digital cameras.

3.2.2 GEMS chamber experiments:

Several recent studies have used New Drill Plus to enhance sediment cohesion in deltaic experiments (Hoyal and Sheets, 2009; Martin et al., 2009; Straub et al., 2015). However, only Kleinhans et al. (2014) attempted to quantify how the polymer influences the shear stress necessary for initiation of sediment motion following sediment deposition. They used a direct shear test to measure the strength of a cohesive sediment mixture. For this type of test, the sample needs to be fully saturated and in well-drained conditions. However, the cohesiveness and low permeability of the sediment mixture prevents the cohesive sediment mixture from draining well. As a result, Kleinhans et al. (2014) found it unsuitable to quantify sediment cohesion from a direct shear test. We attempted to quantify this cohesion using a dual-core Gust Erosion Microcosm System (GEMS) (Gust and Müller, 1997). To do this we conducted an additional experiment with the same forcing conditions as the previously discussed experiments. This experiment included four stages: (1) 60 hours of progradation (2) 80 hours of aggradation with a feed of weakly-cohesive sediment (3) 80 hours of aggradation with a feed of moderately-cohesive sediment and (4) 80 hours of aggradation with a feed of strongly-cohesive sediment. At the end of each

stage, two cores were collected, at least 6.5 cm long, from the deltaic deposits using two 10 cm internal diameter push corers. Immediately following collection of the cores we measured the erodibility of the deposit.

During the GEMS chamber experiments, seven successive shear stresses (0.01, 0.05, 0.10, 0.20, 0.30, 0.45 and 0.60 Pa) were applied to each core and each stress level was maintained steady for about 20 minutes. When the applied shear stress is greater than the critical shear stress of sediment, the sediment surface of the core starts to erode. The eroded materials were suspended and passed through a turbidimeter and collected in bottles. Through filtration of collected turbidity solutions, we measured the eroded mass for each imposed shear stress, which is used to generate eroded mass curves for each experimental sediment mixture.

3.3 RESULTS

In this section, we first present results from the GEMS experiment to characterize the influence of the polymer on sediment cohesion. Next, we statistically characterize how sediment cohesion influences the morphology and dynamics of the depositional system. Our aim is to characterize the full temporal and spatial scales important for autogenic surface dynamics and confirm results from earlier studies that observed a reduction in morphodynamic rates resulting from enhanced cohesion (Hoyal and Sheets, 2009; Edmonds and Slingerland, 2010). Next, we characterize the stratigraphic architecture of each experimental stage. This includes statistical characterizations of stacking patterns, the spatial distribution of fine and coarse

sediment in the deposit, and the volumes of sediment deposited in key depositional environments (channel, terrestrial overbank and marine). Here the goal is to test our hypothesis that changes in morphodynamics induced by cohesion are linked to specific stratigraphic consequences. We test our hypotheses with a suite of statistical metrics which are presented below. For each metric we start by highlighting the surface process or stratigraphic attribute which is being characterized and how this metric will test our core hypotheses. We then present theory which underpins each metric and the methods used to implement the measurements. This is immediately followed by the results of each analysis for our three experimental stages

3.3.1 Erodibility measurement

Several studies note the difficulty in accurately predicting and measuring the erodibility of cohesive sediment (Grabowski et al., 2011; Kleinhans et al., 2014). In this study, we attempt to overcome this through use of a GEMS system. Specifically, we measured eroded mass under each applied shear stress level for each experimental stage (Figure 3.2). In the weakly cohesive stage, the eroded mass increases as the applied shear stress increases. However, the eroded mass curve is almost flat and near zero for the moderately and strongly cohesive stages. These results indicate a significant difference in the erodibility of the weakly cohesive sediment mixture and moderately and strongly cohesive sediment mixtures that include polymer. The structure of the GEMS curves for the moderately and strongly cohesive cases likely indicates that the maximum shear stress level for the GEMS chamber systems is less than that necessary to erode sediments which include the concentrations of polymer

used in our experiments. Although these experiments do not tell the difference in erodibility between the moderately and strongly cohesive sediment mixtures, they do show the presence of polymer in the sediment mixture increases the critical shear stress of the sediment. Given the difficulty in measuring this cohesion and other inherent scaling difficulties, we make no formal attempt to upscale our experiments to field scale, but rather treat them as small systems of and to themselves (Hooke, 1968).

3.3.2 Flow patterns

We start our analysis by noting several qualitative differences in the flow patterns of the three stages. In the weakly cohesive stage rapid lateral spreading of the flow at the entrance to the basin resulted in shallow flow thicknesses. This forced sediment to be transported within several grain diameters of the bed. Similar to previous studies (Kim and Jerolmack, 2008) that utilized weakly cohesive sediment, we observed a morphodynamic cycle characterized by sheet flow deposition which steepened the transport slope followed by the development of an erosional channel. This erosional channel lowered the transport slope and induced channel backfilling, initiating a new cycle of sheet flow and transport slope steepening (Figure 3.3A-C).

The moderately and strongly cohesive experiments were also dominated by a morphodynamic channel cycle. However, this cycle was characterized by the following sequence. Preferential flow paths developed from unconfined flow following channel avulsions. These flow paths developed into channels through a mixture of erosion and aggradation of levees. Channels then prograded into the basin

until a reduced channel slope and deposition of a mouthbar induced a morphodynamic backwater effect (Hoyal and Sheets, 2009). This resulted in channel backfilling until the flow found a weak spot in the channel bank, at which point an avulsion occurred and a new cycle began (Figure 3.3 D-I).

3.3.3 Delta-top area

To test how sediment cohesion affects the partitioning of sediment between terrestrial and marine settings we quantify how the area of each delta changed as a function of the percent of time that area was land, p_{land}. Specifically, we use the topographic maps and our time series of imposed sea-level to extract all land delta-top pixels (elevation > sea-level) for each run-hour. Next, we calculate the percentage of time that each delta-top cell was land. Each terrestrial delta cell is converted to an area equal to 2.5×10^{-5} m^2, determined by the geometry of the imposed topographic grid. Finally, we calculate how the area of the delta changed as a function of the minimum percent of time that area was land.

In our experiments, periods of stable channelization result in large autogenic transgression, as deposition was focused at channel tips in relatively deep water (Figure 3.3 D&G) (Straub et al., 2015). As a result, portions of the delta-top transition between marine and terrestrial environments. On the three curves in figure 3.4 A, the value of delta-top area at p_{land} = 100%, represents the surface area that is above sea level in all DEMs. We note that the area of the delta that is always above sea level, is greatest for the weakly cohesive stage at approximately 1.2 m^2, while this area for the

moderately and strongly cohesive stages are 0.71 m^2 and 0.2 m^2. As p_{land} decreases, the area increases, and the rate of this increase is proportional to the cohesivity of the sediment. As a result, the strongly cohesive stage actually has the largest area that was land in at least one DEM, p_{land} = 1%.

3.3.4 Time scales of surface modification

Similar to previous studies that use overhead images to calculate time scales of channel mobility (Cazanacli et al., 2002; Kim et al., 2010; Straub and Wang, 2013; Wickert et al., 2013), we are interested in characterizing the mobility of the transport systems in our experiments. These earlier studies detail how autogenic mobility is critical for determining the lateral distribution of sediment in basins, time gaps in the stratigraphic record and the response to tectonic forcings. First we characterize the total mobility of the transport system by tracking the fraction of the delta that has experienced geomorphic change (either erosion or deposition) regardless of what environment that change occurred in. Next, we zoom in and characterize the mobility of the channels alone. We do this as one could imagine two deltas with similar total system mobility, one dominated by high lateral channel migration, one dominated by topographic modification through floodplain deposition with slow moving channels. These two cases would likely produce very different stratigraphic architecture and as such determining the mode of system mobility has important implications for stratigraphic prediction, including the distributions and interconnectedness of channel fill deposits.

3.3.4.1 Terrestrial system mobility

Previous studies (Martin et al., 2009; Edmonds and Slingerland, 2010; Caldwell and Edmonds, 2014; Straub et al., 2015) highlight that sediment cohesion can decrease channel mobility. As we are interested in linking cohesion induced changes in the rates of key morphodynamic processes to their stratigraphic consequences, we must first measure how the magnitude of morphodynamic rates varied in our experimental stages. We start by measuring a parameter we refer to as system mobility. Previous experimental studies quantified a similar parameter by tracking the fraction of a delta-top visited by flow in overhead images of the transport system (Cazanacli et al., 2002; Kim et al., 2010; Straub and Wang, 2013). In these experiments sediment was transported mainly as bedload by braided channel systems that lacked overbank flow. As such, it was safe to assume if a region was visited by flow, some geomorphic work occurred. In our experiments, particularly in the strongly cohesive stage, sediment is transported as a mixture of bedload and suspended load and we observe significant overbanking flow, some of which lacked either the shear stresses or sediment concentrations necessary to erode or deposit sediment. Given the high temporal resolution of our topographic data, we decide to measure system mobility directly by measuring the time necessary for significant geomorphic work to occur over a wide swath of the delta-top. We refer to elevation changes, either erosion or deposition, as modifying or regarding the transport surface. We are primarily interested in modification of the terrestrial delta-top, but this introduces a problem, as

our terrestrial delta-top area measurements indicate that shoreline locations autogenically varied through time. As a result, some cells frequently transitioned from terrestrial to marine environments. To compensate for this, we use a constant area that corresponds to the region of each experimental surface that was land for at least 50% of the run time (Figure 3.4B). Here we define f_m, as the fraction of delta-top area modified by a depositional or erosional event of at least 1mm, the vertical resolution of our DEMs. As such, the unmodified fraction (f_{um}) is equal to 1 - f_m. Using our topographic dataset, we track f_{um} by monitoring the fraction of area within our p_{land} = 50% maps yet to be modified for 60 hour windows, starting every 1 hr of run time for each stage. The 60 hr window is long enough for nearly all locations to be modified in each experiment.

The decay of f_{um} in any one stage shows tremendous variability depending on the starting hour. However, when ensemble averaging this variability we find the following results. The average rate of f_{um} decay decreases as sediment cohesion increases, indicating that cohesion reduces lateral system mobility. Second, the variability in f_{um} decay increases as cohesion increases (Figure 3.5A).We explored use of other p_{land} values to characterize system mobility and found that while it changed the absolute value of the measured parameters, it did not change the general trends between experiments.

Similar to Wickert et al. (2013), we fit an exponential trend to each ensemble averaged f_{um} curve (Figure 3.5B):

$$f_{um} = \alpha * \exp(-\lambda_m t) \quad (1)$$

where λ_m is the decay rate, a is a leading coefficient and t is time. The estimated decay rates allow us to characterize a time scale of lateral system mobility, $T_{sy,}$ as the time necessary for 95% of the p_{land} = 50% area to experience topographic modification. This is similar to the channel time scale definition used in previous studies (Cazanacli et al., 2002; Wickert et al., 2013), and represents an important autogenic time scale for deltas. We observe that T_{sy} increases with cohesion and is equal to 15, 30 and 40 hours for the weakly, moderately and strongly cohesive stages, respectively.

3.3.4.2 Terrestrial Channel mobility

System mobility, as defined above, includes mobility that induces geomorphic modification from both channels and overbank flow. Here we isolate the influence of cohesion on just the mobility of channels. This is done to aid our ability to link changes to surface processes induced by cohesion to the partitioning of deposits in channel verses overbank environments. This is accomplished with the topographic scans that were co-registered with digital images of the dyed flow field. The locations associated with active channelized flow were manually mapped for every hour of the three stages (Figure 3.1D). Specifically, we visually identified linear flow features that resembled channel configurations from the digital images collected by the scanner while active dyed flow was turned on. The binary channel maps (1 for channel, 0 for nonchannel) were used to isolate areas modified by channelized flow.

We illustrate the spatial pattern of modification by channels by tracking the time

that each delta-top pixel was first modified by channelized flow, for each experimental stage (Figure 3.6). We do this for the p_{land} = 50% area and over a 300 hr run window for each stage. These maps suggest rapid widespread topographic modification by channels in the weakly cohesive stage and a decrease in channel mobility as cohesion increased.

We quantify the trends observed in Figure 3.6 by tracking the reduction in the fraction of area unmodified by channels, f_{uc}, similar to the method used for measuring f_{um}. Due to large differences in the rate of decay of f_{uc} in each stage, we use 50, 300, and 300 hr windows for the weakly, moderately, and strongly cohesive stages, respectively, starting every 1 hr of run time. These windows are long enough to allow channels to visit most of the p_{land} = 50% area in each stage.

Similar to the f_{um} decay curves, we observe strong variability in the decay of f_{uc}, which increases from the weakly to strongly cohesive stages (Figure 3.7A). To characterize a channel time scale, we fit an exponential trend to the ensemble averaged f_{uc} curves (Figure 3.7B). With the exponential decay rates, λ_c, we estimate the time scale of lateral channel mobility, $T_{ch,}$ as the time necessary for 95% of the p_{land} = 50% area to experience topographic modification by channels. We observe that T_{ch} increases from the weakly to strongly cohesive experiments, which are 16, 164 and 293 hours, respectively.

3.3.5 Experimental Stratigraphy

One of our overarching aims is to link differences in the statistics of the surfaces

processes to statistics that describe stratigraphic architecture. As such, in this section our aim is to link changes in sediment cohesion to qualitative differences in the stratigraphic architecture and quantitative changes in statistics that 1) describe how space is filled in alluvial basins and 2) how sediment of different grain sizes is segregated in the stratigraphy. Given the constant forcing in each stage, differences in the resulting stratigraphy reflect differences in the time and space scales of the autogenic surface processes.

3.3.5.1 Synthetic and physical stratigraphy

We use the topographic data from each experiment to generate volumes of synthetic stratigraphy by stacking DEMs with topography clipped to account for sediment removed during erosional events (Martin et al., 2009). To compare the three experiments, we display the synthetic stratigraphy as a function of a dimensionless mass extraction parameter, χ, which represents the fraction of sediment input to a basin that has been lost to deposition upstream of a distance x (Strong et al., 2005; Paola and Martin, 2012). The volume lost to deposition is the integral of the net rate of deposition r over the area inbound of distance x. Thus, for an initial total sediment flux, Q_s, the value of χ at a given location is equal to:

$$\chi(x) = \frac{1}{Q_S}\int_0^x B(x')r(x')dx' \quad (2)$$

Where B represents the width of a transect at a given distance of x.

In cross-sections of the synthetic (Figure 3.8) and physical stratigraphy (Figure 3.9) from relatively proximal delta-top locations we observe that the strongly cohesive

strata (Figure 3.8C, 3.9A) is mainly composed of coarse channel fill and fine-grained over-bank deposits. Prominent channel levee deposits are noted with high slopes and curvatures. Qualitatively, these levees appear to efficiently segregate the coarse channel body deposits from the fine overbank. Although the moderately cohesive strata (Figure 3.8B, 3.9C) also includes a large number of coarse channel fill deposits, the shape of the levee deposits are flatter compared with those observed in the strongly cohesive stratigraphy (Figure 3.9). The proximal weakly cohesive deposit (Figure 3.8A, 3.9C) is dominated by flat lying time lines and by bedload deposits with a broad range of grain sizes intermixed. This deposit also has several large stacked coarse channel deposits in the middle of the cross-sections that are the result of short lived incisional channels. Similar trends are seen in the three distal transects (Figure 3.8D-F, 3.9B&D), except that sandy channel deposits are largely replaced by sandy lobe deposits. Again, the segregation of fine from coarse sediment qualitatively appears to increase as the cohesion is increased.

3.3.5.2 Compensation metric

Overhead images and results from our statistical description of the surface dynamics indicate that sediment cohesion increases the tendency for channels to lock in place for long periods of time. We hypothesized that an increase in the stickiness of channels should increase the persistence in deposition trends in the stratigraphic record and reduce the evenness of basin fills over a range of time scales. To test these hypotheses we use the compensation statistic, which compares sedimentation patterns

to the pattern of the long term generation of accommodation. Compensation describes the tendency of deposits to preferential fill topographic lows in the transport system. Straub et al. (2009) linked compensation in basin filling to the decay of the spatial variability in sedimentation between select depositional horizons as a function of increasing vertical stratigraphic averaging distance.

The variability in sedimentation patterns is quantified using the standard deviation of the ratio of sedimentation over a time window of interest to the long term sedimentation rate (Sheets et al., 2002):

$$\sigma_{ss}(T) = \left(\int_A \left[\frac{r(T;x,y)}{\hat{r}(x,y)} - 1 \right]^2 dA \right)^{1/2} \qquad (2)$$

where r is the local sedimentation rate measured over a temporal stratigraphic interval T, x and y define horizontal coordinates, A is the area over which the calculation is performed, and $\hat{r}$ is the local long-term sedimentation (or subsidence) rate. Over long time windows, transport systems have a tendency to visit every spot in a basin repeatedly. Thus, the ratio of sedimentation to subsidence at any point in the basin should approach unity in the limit of time. However, over short time windows, depositional geometries within the basin are controlled by the configuration of the transport system. Consequently, the ratio of sedimentation to subsidence over these time scales is variable.

When calculating $\sigma_{ss,}$ we use DEMs of surface topography rather than preserved stratigraphic horizons. As a result, our estimates of σ_{ss} are built from the full distribution of paleo-surface processes and include ratios of short term sedimentation rate to long term rates that can be both negative (erosion) and positive (deposition).

Here we note that use of surface topographic data will likely produce slightly higher estimates of σ_{ss} than produced from stratigraphic surfaces, where only preserved deposition can be measured.

Similar to Wang et al. (2011), we observe that the slope of the decay of σ_{ss} as a function of measurement time is scale dependent (Figure 3.10). Previous studies showed that the exponent of this power law decay, the compensation index (κ), describes the tendency for deposits to stack compensationally, with increasing κ values associated with stronger compensation. From our plots of σ_{ss} as a function of measurement window, we make the following observations. 1) Regardless of the time window of interest, the variability in the depositional patterns, as quantified with σ_{ss} goes up as cohesion increases. This suggests larger autogenically induced variability in stratigraphic stacking patterns of cohesive systems, which is in agreement with our qualitative observations. 2) The variability of σ_{ss} for a given time window increases as sediment cohesion increases. 3) Over short time scales the decay rate of σ_{ss}, and thus κ, is greatest for the weakly cohesive case and decreases as sediment cohesion increases. This indicates that, over shorter time scales, the strength of compensation decreases as sediment cohesion increases. Over longer measurement windows this decay rate approaches 1 for all stages, which indicates complete compensation as depositional patterns match the pattern of accommodation generation. Wang et al. (2011) highlighted that the time scale associated with complete compensation, termed the compensation time (T_c), represents the upper limit of autogenic time scales in basin filling and can be estimated as the maximum scale of autogenically induced

roughness on a transport system divided by the long term, basin wide aggradation rate. A point we will return to in the discussion.

3.3.5.3 Spatial composition variability of physical stratigraphy

Understanding controls on the magnitude and spatial scales of compositional changes in stratigraphy has implications for prediction of stratigraphic properties, including the connectivity of high permeability zones. While results from our analysis of compensation indicate cohesion induced changes in the filling of accommodation, the metric used did not quantify the spatial variability of deposit composition. Here we tackle this question using a metric which quantifies segregation of fine and coarse particles over a range of spatial scales. To accomplish this we use spatial changes in the intensity of color in the physical stratigraphic sections as a proxy for the spatial composition variability. We use the three color bands, R, G, B, captured by digital images of the stratigraphy to calculate the red intensity in each pixel of the deposits:

$$I = \frac{R - G - B + 2 * C_{\max}}{3 * C_{\max}} \quad (3)$$

where C_{max} is the maximum possible value for each color band and here is equal to 255.

To quantify segregation by particle size, we measure the coefficient of variation, *CV*, of the sediment color intensity in square measurement windows over the extent of each stratigraphic panel. For a given measurement window, *CV* is calculated as:

$$CV = \frac{\sqrt{\frac{1}{N}\sum_{i=1}^{N}(I_i - \bar{I})^2}}{\bar{I}} \quad (4)$$

where N is the total number of square measurement windows of a specified size within the stratigraphic panel of interest, $\bar{I}$ is the mean normalized color intensity, and I_i is the normalized color intensity in each square measurement window of the panel. We then track how CV varies as a function of the size of a measurement window (Figure 3.11). We do this calculation for windows with sizes ranging from 10 by 10 image pixels (~1.5×10^{-5} m^2) to ~0.015 m^2.

Qualitatively, we noted that an increase in cohesion resulted in the separation of fine (white) from coarse (either red or blue) sediment. As cohesion increased the fines were largely sequestered in overbank deposits while the coarse material dominantly was stored in channel fill and lobe deposits (Figure 3.9). Quantitatively, if strong segregation of fine and coarse material is present there will be locations with high color intensity (sandy material) and locations with low color intensity (fine material). As a result, the CV of these intensities would be high. If segregation is minimal, most windows, at the measurement size of interest, will have roughly the same intensity and CV will be low. Over small measurement windows, we observe that CV of the stratigraphy increases as the cohesion of the sediment increases for both the proximal and distal sections (Figure 3.12). The ordering of CV between stages for the proximal section is dependent on the window size. At a window size approximately equal to 240 mm^2 the CV of the three experiments converges and a larger window sizes the ordering of stages is reversed relative to what is observed at small window sizes. We note that this window size is approximately the scale of the channel sand bodies in the three experiments, suggesting that the qualitative segregation we observe largely

happens at scales finer than a channel sand body. We also note that if the same ratio of fine to coarse material exists in two sections, they should have equal *CV* measurements at window sizes that are, at a minimum, the size of the deposit.

3.4 DISCUSSION

3.4.1 Influence of sediment cohesion on surface dynamics: System and channel mobility numbers

In this study, we systematically quantify how an increase in sediment cohesion influences the time and space scales of deltaic autogenic processes. While our GEMS experiments could not differentiate the erodibility of the moderately and strongly cohesive sediment mixtures, our statistical characterization shows clear differences between the three stages. One of the major findings in the surface dynamics is that an increase of sediment cohesion reduces both system and channel lateral mobility and thus increases the autogenic time scales necessary to regrade the deltaic topography, through channels or a combination of both channelized and overbank flow. This observation is consistent with previous studies, which note that sediment cohesion promotes channelization and decreases channel lateral mobility (Martin et al., 2009; Edmonds and Slingerland, 2010; Caldwell and Edmonds, 2014; Straub et al., 2015).

To further explore how sediment cohesion influences system and channel mobility and link these dynamics to possible stratigraphic architectures, we define two non-dimensional numbers that compare the lateral mobility to vertical mobility over basin-filling time scales. Specifically, we define a basin filling system mobility

number, M_s, and a basin filling channel mobility number, M_c as:

$$M_s = \frac{h/v}{T_{sy}} = \frac{T_c}{T_{sy}} \quad (5)$$

$$M_C = \frac{h/v}{T_{ch}} = \frac{T_c}{T_{ch}} \quad (6)$$

where h is the maximum autogenic roughness length of the transport system, v is the basin-wide long-term aggradation rate, and T_c is the compensation time scale, or the time necessary to aggrade, on average, one vertical roughness scale everywhere in the basin (Wang et al., 2011). The spirit behind M_c and M_s is similar to a short-time scale mobility number proposed by Jerolmack and Mohrig (2007), who compare the time necessary for a single channel to aggrade one channel depth to the time necessary to laterally migrate one channel width.

We are interested in relating M_s and M_c to characteristics of the stratigraphic architecture. We note that M_s, by itself, is not particularly useful in predicting stratigraphic architecture. We can imagine two systems with equally high mobility, one coming from rapidly migrating channel bodies with limited overbank deposition and a second system defined by slow moving channels, but frequent overbanking flow that is able to modify floodplains. Similar to the short-time scale mobility number of Jerolmack and Mohrig (2007), we propose that the relative magnitude of M_c is related to the propensity of channel deposits to contain evidence for vertical vs. lateral migration. As such, systems defined by high M_c should have channel deposits with widths much greater than the channels that deposited them, while channel bodies of low M_c systems will have channel body widths of similar magnitude to their

paleo-channel forms. Finally, we propose that while the value of M_s on its own might not greatly aid stratigraphic prediction, the ratio of M_c to M_s is related to the relative fraction of channel to overbank deposits in the preserved record.

To estimate either of our mobility numbers, we first must measure h. To do this we detrend each topographic map for the long-term basin-wide deposition rate imposed by the base-level rise. Next, we detrend each map for the long-term average spatial structure of topography. This second step is necessary as the migration of channels over the delta top, originating at the basin infeed location at the center of the proximal wall, resulted in an average symmetric convex up profile of topography for all strike oriented transects, with on average the highest topography located in the center of the basin. In addition, to drive transport sediment towards the ocean, an average down system slope was present that must be accounted for prior to estimating h. We define h as the difference of the 97.5 and 2.5 percentiles of the detrended elevation distribution. We find that this roughness length scale, and thus the compensation time scale, increases as sediment cohesion increases (Figure 3.12 A). T_c has been defined as the maximum autogenic time scale in basin filling (Wang et al., 2011). As such, our results indicate that increasing sediment cohesion increases both the time scales of autogenic lateral mobility and autogenic space filling. Thus, our basin filling mobility numbers allow us to examine if lateral mobility decreases faster than vertical space filling mobility as cohesion is increased.

The estimates for T_c allow us to calculate M_s and M_c for each stage (Figure 3.12 B and C). We find that increasing sediment cohesion actually increases M_s in our

experiments, suggesting that addition of cohesion causes the vertical space filling mobility to decrease faster than the decrease observed in lateral system mobility. Put another way, the trend in M_s indicates that increasing sediment cohesion resulted in a stronger response to the growth of surface roughness (i.e. channel deepening) than the commensurate decrease in lateral mobility.

As expected, the increase in cohesion is associated with a significant decrease in the channel mobility numbers over basin filling time scales. Combined, the trends in M_s and M_c suggest that while increasing sediment cohesion slows the movement of channels, it also results in deeper channels with faster moving flow that can pump suspended sediment to overbank environments where it can modify topography. We also see that M_c for the moderately and strong cohesive stages is significantly less than 1, meaning that over the course of 1 T_c channels generally do not visit all basin locations. Coupling this with the significant system mobility attributed to overbank activity should result in stratigraphy dominated by isolated channel bodies with widths that are similar to their geomorphic forms and isolated channels that are incased in overbank deposits. These predictions match observations of the architecture observed in our physical stratigraphic panels.

3.4.2 Linking deltaic surface dynamics with subsurface stratigraphy

Straub et al. (2015) use the same set of experiments discussed here to show how sediment cohesion increases scales of autogenic shoreline transgressions and regressions and how this could influence the scales of autogenic parasequences. We

find that an increase in sediment cohesion also increased the variability of depositional patterns relative to the generation of accommodation. This enhanced variability is the result of strong depositional persistence induced by a reduction in the lateral mobility of both the system and channels due to cohesion. Here we explore if this increase in depositional persistence is correlated with changes in the volume of sediment preserved in stratigraphy from various depositional environments. To accomplish this we use the channel maps and synthetic stratigraphy to measure the fraction of the stratigraphy deposited in terrestrial channels, terrestrial overbank, and marine environments, relative to the total volume of sediment input to the basin. We first use the synthetic stratigraphy to calculate sediment volumes preserved between two consecutive scans. Next, using our maps of channel locations and the imposed sea level, we separate this volume into our three depositional environments. Unfortunately, deep ocean water depths in later parts of our experiments prevented us from measuring topography for most of the marine environment. We did observe a large volume of pro-delta sediment when draining and cleaning the basin after each experiment. Given our near universal coverage of terrestrial settings, we assume that any sediment input to the basin, which is not accounted for in our synthetic stratigraphy, was deposited in marine environments.

With our final inventory of sediment volumes from each depositional environment, we make the following observations. As sediment cohesion increased, the fraction of sediment deposited in the terrestrial (channel + overbank), decreased from the weakly to strongly cohesive stages (Figure 3.13&3.14). This is consistent

with the results of Straub et al. (2015) who found that an increase in sediment cohesion decreased deltaic retention rates.

Second, the fraction of channel deposits decreased from the weakly to strongly cohesive stages (Figure 3.13). This likely indicates that cohesion led to fewer channels that had lower lateral mobility and thus less capacity to rework floodplain deposits into channel deposits and/or that the reduction in lateral channel mobility was linked to an increase in suspended sediment laden flow to the overbank environment. These two processes are likely the mechanisms responsible for the increased segregation of fine from coarse sediment observed with increasing cohesion. In section 3.3.4 we proposed that the ratio of channel to system mobility could be linked to the ratio of channel to overbank deposits. Here we explore this by comparing the decay rate of modified area by channels to the decay rate of area modified by the total transport system:

$$\lambda_n = \frac{\lambda_c}{\lambda_m} \qquad (4)$$

. Supporting our hypothesis, we find that a decrease in λ_n is linked to a reduction in channel fill deposits in our experiments (Figure 3.15).

Finally, we note that the volume of terrestrial overbank deposits increased from the weakly cohesive to moderately cohesive stage but then decreased for the strongly cohesive stage. We hypothesize that this trend is related to the change in delta size between stages. It is possible that overbanking flow increased progressively as sediment cohesion increased. However, the small delta area in the strongly cohesive case allowed some sediment transported out of channels to be advected to the marine

prior to deposition, thus resulting in marine deposition. Combined, these measurements and observations suggest that sediment cohesion can have a strong impact both on the terrestrial sediment retention rates and on the volume of sediment deposited in channel relative to overbank settings.

3.5 SUMMARY

Using physical experiments, we examine the influence of sediment cohesion on the temporal and spatial time scales of deltaic surface dynamics and how these surface processes set stratigraphic architecture over basin-filling time scales. Building on previous studies, we use metrics to quantify how the addition of cohesion influences key autogenic process and product scales. The main results are summarized as follows:

1. Sediment cohesion promotes the development of deep, laterally stable channels. The low lateral mobility of cohesive systems reduces the capacity to laterally distribute sediment. As a result, the temporal and spatial scale of autogenic shoreline transgressions increases with cohesion. This reduces the area of deltas that is consistently above sea-level.
2. Using topographic data and maps of channel locations, we calculate an autogenic time scale for topographic modification and a time scale for modification by channels in each experimental stage. The first time scale is set by the lateral mobility of the total transport system (overbank + channels) while the second is set just by the lateral mobility of channels. Increasing

sediment cohesion is linked to a reduction in lateral mobility of both the total transport system and the channels. However, the reduction in lateral channel mobility is greater than that of the total system, indicating that sediment cohesion aids the pumping of sediment laden flow to overbank settings where it can modify topography and fill space.

3. Depositional time lines in volumes of synthetic stratigraphy, generated from topographic data clipped for erosion, indicate that cohesion enhances depositional persistence. This enhanced persistence reduces the match between patterns of deposition and patterns of accommodation generation over a wide range of time scales. This suggests a link between autogenic time scales that quantify surface mobility and the autogenic scales present in stratigraphy.
4. Observations of the experimental physical stratigraphy suggest that cohesion increases the segregation of coarse material into channels and lobes while the fine material is segregated into overbank deposits. This segregation is linked to a decrease in the total volume of channel relative to overbank deposits in the preserved record.

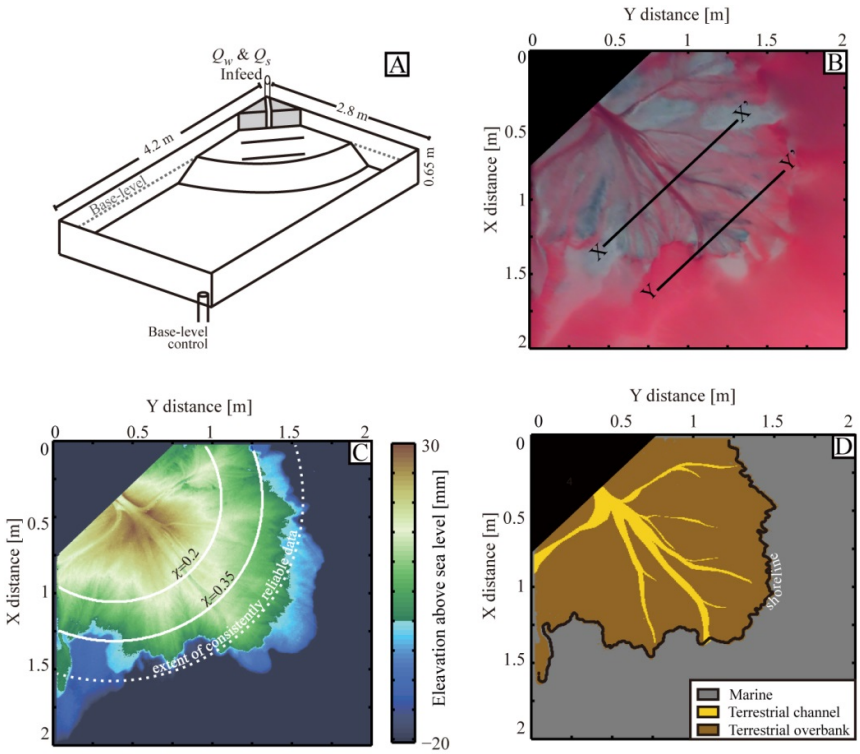

Figure 3.1 Schematic of experimental setup and maps illustrating types of data collected over the course of each experimental stage. A) Schematic diagram of Tulane Delta Basin with key basin dimensions and controls labeled. B) Characteristic digital image of the moderately cohesive experiment with flow on and dyed for visualization. Image collected with laser scanner such that all pixels are referenced relative to the basin coordinate system. Location of physical stratigraphic sections are shown by solid black lines. C) DEM of experimental surface collected with laser scanner. Location of synthetic stratigraphic sections from figure 8 are shown by solid white lines. Dashed white line shows the extent of DEMs where topography was reliably measured for each run hour. D) Map of depositional environment. Channel locations were manually mapped from digital images and coupled to topography and sea level history to define three environments. Solid black line denotes shoreline.

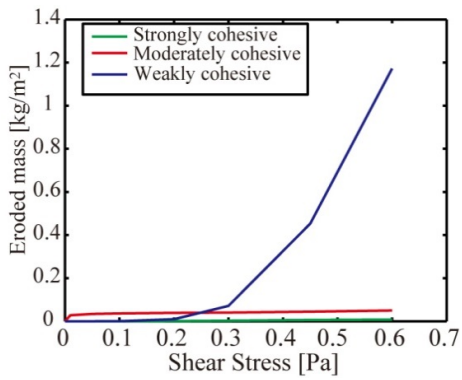

Figure 3.2 Measurements of eroded mass due to increasing applied shear stress to cores of experimental deposits in a GEMS Chamber experiment.

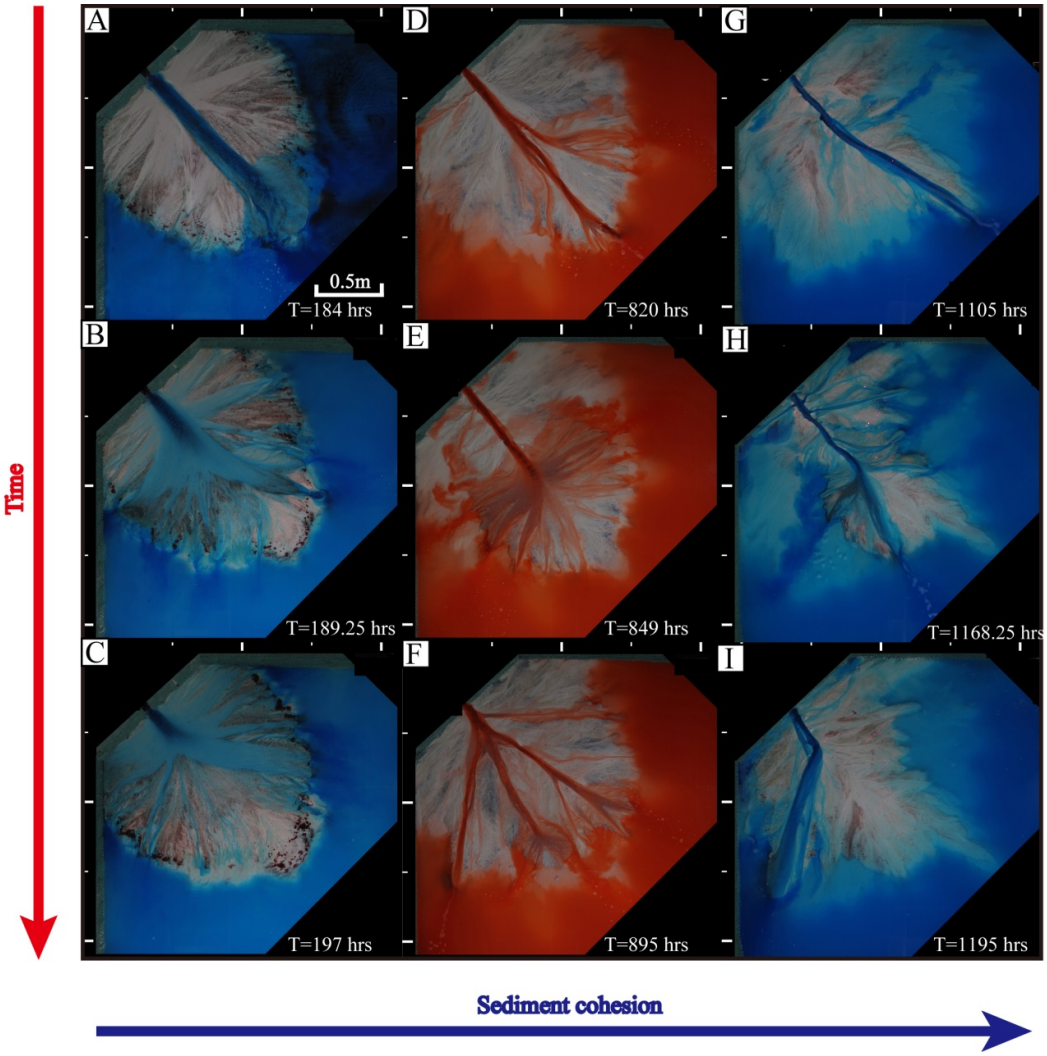

Figure 3.3 Overhead images of the three experiments. Each experiment experienced repeated cycles of autogenic channel formation, back stepping, and avulsion. As cohesion increased this process occurred over longer time scales, channel lateral mobility decreased, and shoreline variability increased.

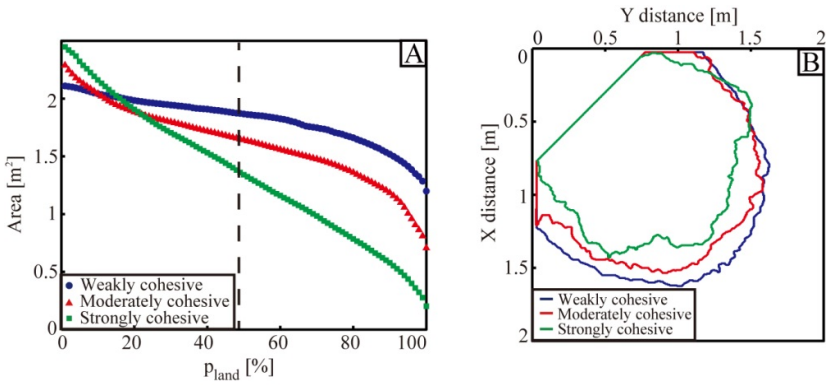

Figure 3.4 Data defining (A) the experimental area that was above sea-level for different percentages of run-time in the three experimental stages and (B) the shape of the delta area that was land for at least 50% of each experimental stage.

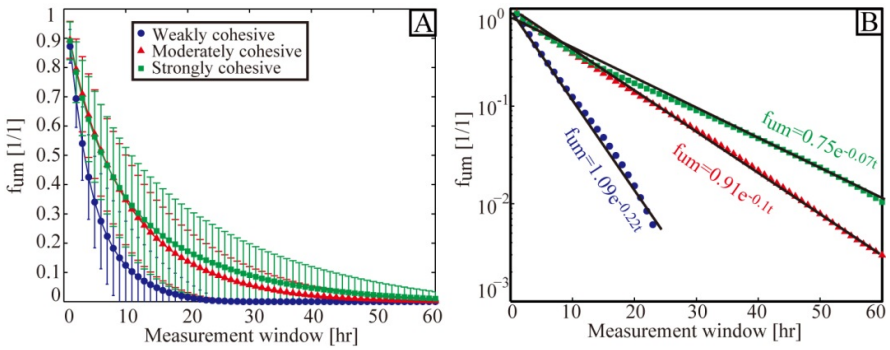

Figure 3.5 Data defining the reduction in area that has not experienced topographic modification. (A) Data in arithmetic, arithmetic space with mean decay trend represented by symbols. Vertical bars represent variability in measurements and are equal to +/- one standard deviation. (B) Decay of mean trend in semi-log space to illustrate approximate exponential reduction in f_{um}. Equations of best-fit trends lines are also shown.

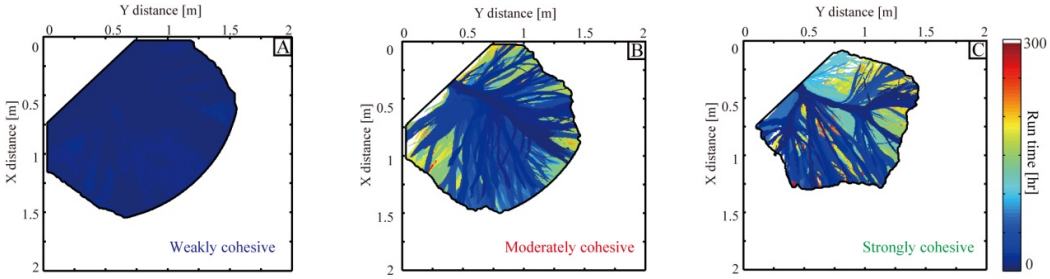

Figure 3.6 Locations modified by river channels through time. The solid lines in A-C represent the shape of the delta area that was land for at least 50% of each experimental stage.

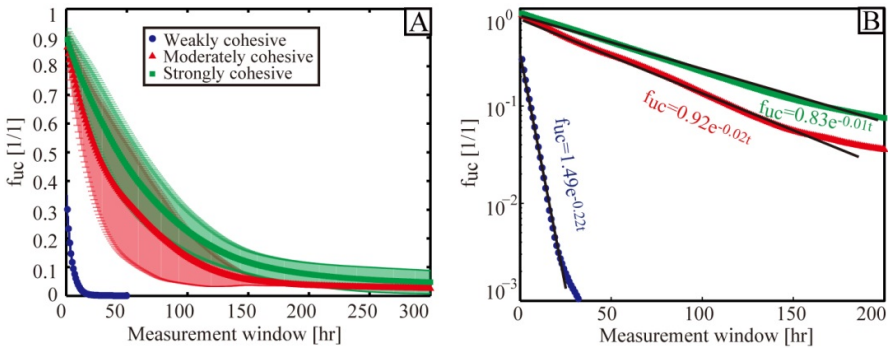

Figure 3.7 Data defining the reduction in area that has not been modified by channelized processes. (A) Data in arithmetic, arithmetic space with mean decay trend represented by symbols. Vertical bars represent variability in measurements and are equal to +/- one standard deviation. (B) Decay of mean trend in semi-log space to illustrate approximate exponential reduction in f_{uc}. Equations of best-fit trends lines are also shown.

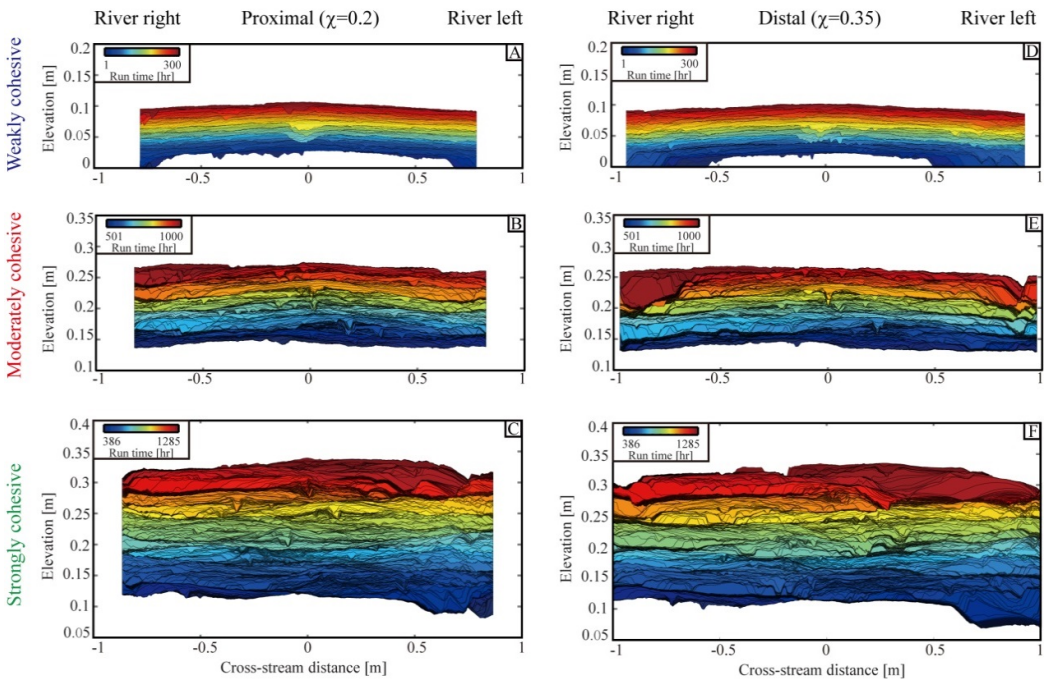

Figure 3.8 Synthetic stratigraphy along proximal (A-C) and distal (D-F) delta-top strike oriented transects. Transects are located at equivalent mass extraction locations in each experiment corresponding to $\chi = 0.2$ and $\chi = 0.35$ for the proximal and distal transects, respectively. Location of transects for moderately cohesive case are shown in figure 1C. Stratigraphy is colored by time of deposition in each experiment and lines represent topography clipped for erosion.

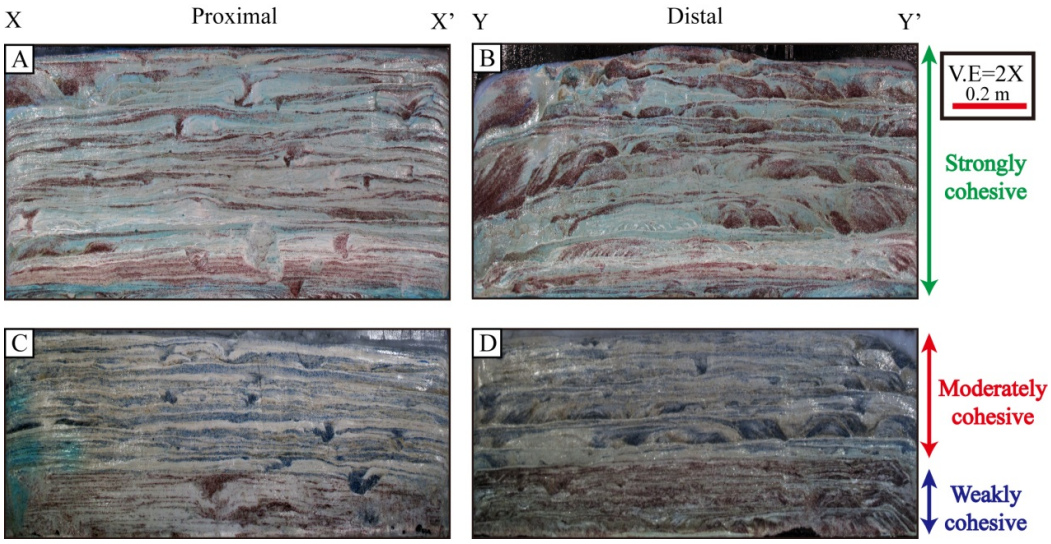

Figure 3.9 Images of preserved physical stratigraphy of the three experimental stages from a proximal (A&C) and distal (B&D) strike oriented transect. Panels are oriented as if one were looking down system. Location of transects are shown in figure 1B.

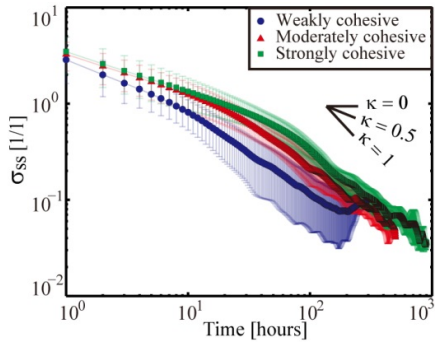

Figure 3.10 Comparison of the decay of σ_{ss} as a function of time window of measurement for the three experimental stages. Vertical bars represent variability in σ_{ss} measurements and are equal to +/- one standard deviation.

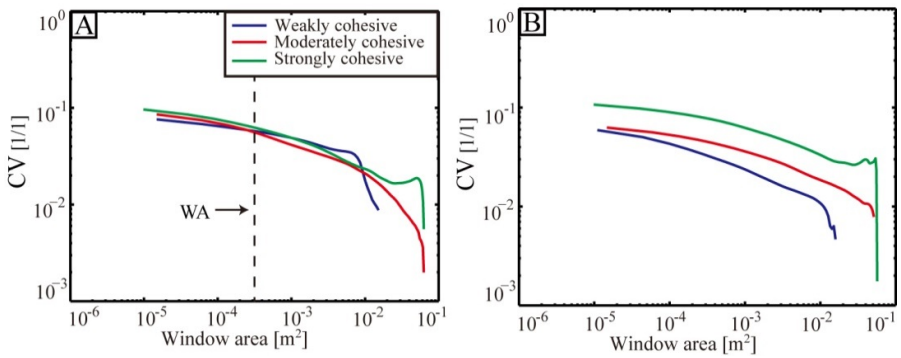

Figure 3.11 Comparison of stratigraphic spatial variability in composition as expressed by *CV* for increasing measurement window area in the three experimental stages for the (A) proximal and (B) distal physical stratigraphic panels.

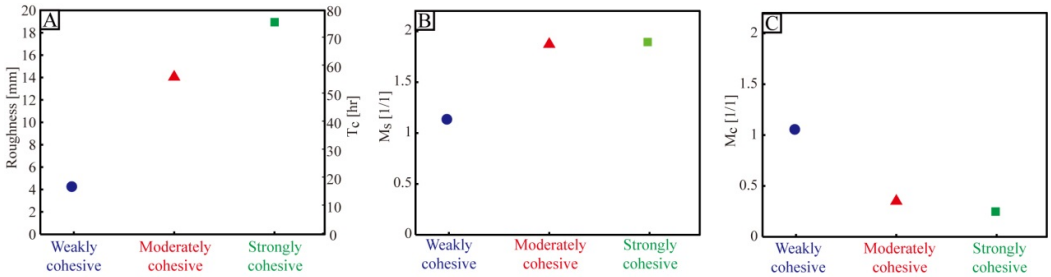

Figure 3.12 Measurements of (A) deltaic roughness and associated calculation of compensation time which are used to measure the system (B) and channel (C) mobility numbers over basin filling time scales for the three experimental stages

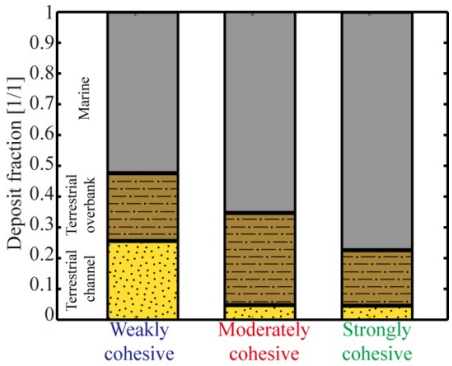

Figure 3.13 Percent of stratigraphic volume deposited in terrestrial channel, terrestrial overbank, and marine environments in the three experimental stages.

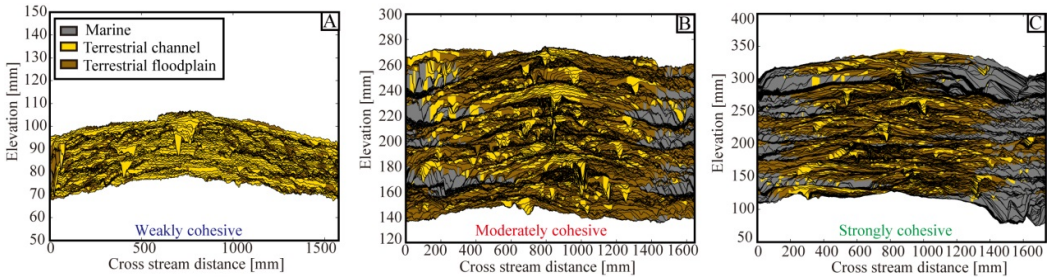

Figure 3.14 Synthetic stratigraphy along the proximal delta-top strike oriented transect. Transects are located at equivalent mass extraction locations in each experiment corresponding to χ = 0.2. Location of transect for moderately cohesive case is shown in figure 1C. Stratigraphy is colored by environment of deposition and lines represent topography clipped for erosion.

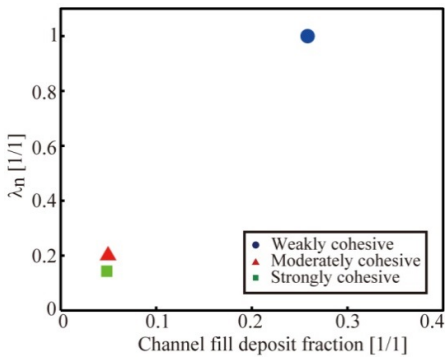

Figure 3.15 Relationship between ratio of channel to system lateral mobility and the fraction of a deposit composed of channel fill.

Chapter 4

Storage Thresholds for Relative Sea Level Signals in the Stratigraphic Record

ABSTRACT

The tug of Relative Sea Level (RSL), set by climate and tectonics, is widely viewed as the most important boundary condition for the evolution of deltas. However, the range of amplitudes and periodicities of RSL cycles stored in deltaic stratigraphy remains unknown. Experimental results presented here suggest that extraction of RSL cycles from the physical stratigraphic record requires their magnitudes and periodicities to be greater than the spatial and temporal scales of the internal (autogenic) dynamics of deltas. These results predict stratigraphic storage of information pertaining to RSL cycles during icehouse Earth conditions. However, these thresholds often overlap with the magnitudes and periodicities of RSL cycles for major river deltas during greenhouse Earth conditions, which suggest stratigraphic signal shredding. This theory suggests quantitative limits on the range of paleo-RSL information that can be extracted from stratigraphy, which could aid the prediction of deltaic response to climate change.

4.1 INTRODUCTION

Since the work of Gilbert (1890), a plethora of studies have examined how Relative Sea Level (RSL) change influences the production of stratigraphic surfaces (e.g. sequence stratigraphy) and stratigraphic patterns (e.g. alluvial architecture) (Vail et al., 1977; Van Wagoner et al., 1990; Blum and Törnqvist, 2000; Martin et al., 2009; Karamitopoulos et al., 2014). This has led many to argue that RSL change represents the most important boundary condition (allogenic forcing) affecting deltas and is the primary control on stratigraphic architecture. RSL change, defined as the sum of local absolute sea level rise and subsidence rates, is driven by a range of processes. These span small magnitude and short period cycles (mm's of change over days) driven by atmospheric dynamics to the large magnitude and long period cycles (100's of m's of change over 100's of millions of years) resulting from plate tectonics (Miller et al., 2005). Are all of these RSL cycles stored in stratigraphy and if not, what attributes must a cycle have for storage to occur? Answering this question requires development of quantitative theory and rigorous methods to test proposed thresholds, which is the focus of this work.

While much work highlights the response of deltas to allogenic forcings, we have less theory for prediction of autogenic dynamics and their stratigraphic products (Hoyal and Sheets, 2009). A suite of recent numerical experiments do examine the deposits of autogenic processes (Dalman et al., 2015) and how they interact with Quaternary scale RSL cycles (Karamitopoulos et al., 2014), but at present we lack a quantitative framework to define how other cycle periods and magnitudes interact

with autogenic processes. Results from a recent study by Jerolmack and Paola (2010), from here on referred to as JP2010, suggest that autogenic processes can alter, or in some cases shred, sediment flux signals during their propagation from source to sink. By shredding, Jerolmack and Paola mean a smearing of an input signal over a range of time scales such that the signal is not detectable at the outlet of a system. The JP2010 theory suggests that when the scale of an input signal is less than the scale of a system's autogenic processes they are prone to shredding. While the JP2010 theory makes important quantitative predictions, it does not define conditions necessary for stratigraphic storage, as they were primarily interested in sediment flux time-series. Motivated by JP2010, we aim to define stratigraphic storage thresholds for RSL change, in contrast to the transport thresholds of JP2010.

4.2 HYPOTHESIZED STORAGE THRESHOLDS

We hypothesize that the upper spatial and temporal limits of autogenic processes influence the storage of RSL cycle information in stratigraphy. We define the upper spatial limit of autogenic processes as the depth of the largest channels, H_c, as post-avulsion incision results in the greatest elevation changes. Next, we define the upper temporal limit of autogenic processes using the compensation time scale, T_c, which scales with the time for the shape of a deposit to solely be influenced by boundary conditions (i.e. subsidence patterns) (Wang et al., 2011). This time scale can be estimated as $H_c/\bar{r}$, where $\bar{r}$ equals the long term aggradation rate. Thought of in another way, T_c represents the time necessary for a particle deposited at the Earth's surface to be buried to a depth that is no longer susceptible to remobilization from

autogenic incision events.

We define two non-dimensional numbers which compare the upper spatial and temporal scales of deltaic autogenic processes to the magnitude and periodicity of RSL cycles:

$$H^* = \frac{R_{RSL}}{H_C} \tag{1a}$$

$$T^* = \frac{T_{RSL}}{T_C} \tag{1b}$$

where R_{RSL} is the range of a RSL cycle (i.e. difference in elevation from cycle peak to trough) and T_{RSL} is the period of a RSL cycle. We hypothesize that deltas experiencing RSL cycles characterized by H^* and/or $T^* >> 1$ will store RSL cycle information in stratigraphy. However, information associated with RSL in settings where both H^* and $T^* << 1$ will be shredded.

4.3 EXPERIMENTAL METHODS

We investigate storage of RSL cycles in stratigraphy using reduced scale physical experiments that allow stratigraphic products to be directly linked to surface dynamics (Hoyal and Sheets, 2009; Martin et al., 2009). Experiments were conducted in the Tulane University Delta Basin, which is 4.2 m long, 2.8 m wide, and 0.65 m deep. First, we performed a control experiment to characterize the range of deltaic autogenic time and space scales (Figure 4.1A). This experiment had constant water supply ($Q_{w,input}$ = 1.7 x 10^{-4} m^3/s), sediment supply ($Q_{s,input}$ = 3.9 x 10^{-4} kg/s), and a constant sea level rise rate ($\bar{r}_{SL}$ = 0.25 mm/hr) which promoted the deposition of ~18

channel depths of stratigraphy. The constant $\bar{r}_{SL}$ mimics a spatially uniform relative subsidence pattern. Long-term sea level rise rate was set to balance accommodation creation and input sediment supply. The input sediment mixture was designed to mimic earlier experimental work (Hoyal and Sheets, 2009) and had a broad distribution, ranging from 1 – 1000 μm with a mean of 67 μm, and included a small amount of a polymer to enhance sediment cohesion. While the majority of the sediment was white in color, a fraction of the coarse tail of the distribution was replaced with dyed sediment of near equivalent size to aid visualization of stratigraphic architecture. The input water was dyed with a food coloring to aid characterization of morphodynamics.

Topography was monitored once an hour with a laser scanner, resulting in digital elevation models with a 5 mm grid in the down and cross basin directions, respectively. The high temporal and spatial data resolution allow us to generate synthetic stratigraphic panels through the stacking of sequential scans, clipped for erosion (Martin et al., 2009). Finally, we collected digital images of the active delta top every 15 minutes.

We test the validity of our RSL cycle stratigraphic storage thresholds using experiments that share the same boundary conditions as the control experiment, with the exception of RSL cycles that vary in magnitude and periodicity between experiments. Here we focus on three experiments with cycles characterized by either 1) $T^* > 1$, but $H^* < 1$, 2) $H^* > 1$, but $T^* < 1$, or 3) H^* and $T^* < 1$.

4.4 RESULTS

Starting with the surface dynamics, we search for the signature of RSL cycles in time series characterizing channel mobility. Most theory suggests a reduction of channel mobility during falling RSL associated with topset incision (Van Wagoner et al., 1990). We use changes in the intensity of deltaic surface color as a proxy for the magnitude of channel mobility in the experiments. Intervals with high channel mobility occur when significant areas of the delta switch from being covered by dyed flow to being covered by dry white sediment or vice versa. We use the three color bands (RGB) captured in digital photographs of the active deltaic surface captured once an hour to characterize channel mobility along a proximal transect (Figure 4.1A-B). For intervals when the flow was dyed blue, dye intensity is calculated as the magnitude of B-R-G, while dye intensity is calculated as R-B-G when the flow was dyed red (Figure 4.1C). In addition to quantifying surface dynamics, channel mobility influences field scale stratigraphy as it is inversely correlated to paleosol development. We then generate time series of the mean value of the absolute change in dye intensity along the transect for each measurement hour (Figure 4.1D), which are used to generate power spectra. Next, we produce confidence bands for the identification of statistically significant periodicities by performing a Chi-square test on the power spectra of our control experiment. We find statistically significant peaks at the periodicity of imposed RSL cycles in experiments with H^* or $T^* > 1$. No peak is observed in the experiment where H^* and T^* were both < 1 (Figure 4.1E-H).

Next we search for the signature of imposed RSL cycles in the experimental

stratigraphy. We generate time series of mean deposition rates, $\overline{\partial\eta/\partial t}$, from synthetic stratigraphic panels oriented perpendicular to the mean flow direction (Fig 4.2A-H). Similar to our analysis of channel mobility, we find statistically significant peaks at the periodicity of imposed RSL cycles in the stratigraphy of experiments with H^* and/or T^* values >= 1. However, no statistically significant peak is observed in the stratigraphy of the experiment where H^* and $T^* < 1$ (Figure 4.2I-L): a result consistent with our primary hypothesis.

As the signature of RSL cycles has been linked to many stratigraphic attributes, we performed additional analysis. These include time series analysis of the second moment of deposition rates, similar in spirit to the regional stratigraphic variability defined by Karamitopoulos et al. (2014). Results of this test are consistent with our analysis of channel mobility and mean deposition rates. Analysis of the facies architecture also suggest no significant differences between our control and low H^* low T^* experiments, while significant differences in the width-to-depth ratio of channel bodies and deposit sand fraction exists between the control and non-shredded experiments. Additional experiments were performed which further explore the T^* vs. H^* phase space and support the above findings (see Appendix to chapter 4).

To explore the significance of the experimental results, we compile a database of H_c and T_c for field scale deltaic depocenters (Figure 4.3). Calculation of T_c is done with $\bar{r}$ values measured over time scales in excess of 100 kyrs. (LINDSAY et al., 1991; Jerolmack and Sadler, 2007) show that for deltas this time scale is necessary for persistence in deposition rates as a function of measurement interval to be achieved.

These values are compared to Milankovic scale RSL cycles in the Middle Pleistocene – present when eccentricity cycles (~100 kyr) resulted in RSL changes of ~100 m. We also compare our database to Late Miocene conditions when obliquity cycles (~40 kyr) resulted in RSL changes with ranges of 10-35 m. Our results show that R_{RSL} of Middle Pleistocene – present cycles exceeds H_c of almost all compiled systems, while the T_{RSL} of eccentricity cycles is not consistently less than or greater than our estimates of T_C. Exploring Late Miocene conditions we make the following observations: 1) The R_{RSL} and T_{RSL} of RSL cycles during this period are in excess to the autogenic scales of smaller systems like the Rhine or Rio Grande Deltas, 2) Large systems, such as the Ganges-Brahmaputra and Mississippi Deltas, have autogenic spatial and temporal scales greater than Late Miocene RSL cycles, 3) Finally, the autogenic scales of the majority of systems in our compilation lie close to scales of Late Miocene RSL cycles.

4.5 DISCUSSION

To illustrate the importance of our proposed thresholds we use our data base of channel depths and compensation time scales to make predictions of RSL signal storage in icehouse and greenhouse Earth conditions (Miller et al., 2005). We use Icehouse Earth to refer to periods with waxing and waning of continental scale ice sheets, while greenhouse Earth refers to periods with no continental scale glaciers and thus small magnitude Milankovic forced RSL cycles. We use attributes of RSL cycles in the Middle Pleistocene – present to examine icehouse Earth conditions and

attributes of Late Miocene RSL cycles to represent greenhouse Earth conditions. While the Late Miocene did have ice sheets, we use it due to our high precision knowledge of small magnitude sea level fluctuations during this period, similar to greenhouse Earth RSL cycles.

Starting with icehouse Earth conditions: we note that the range of these RSL cycles far exceed the depth of almost all channels explored, suggesting signal storage. This finding is supported by the vast number of geomorphic and stratigraphic observations (Blum and Törnqvist, 2000) linked to recent RSL change. Exploring greenhouse Earth conditions, we predict signal storage in small systems, such as the Rhine or Rio Grande Deltas. However, we predict that these same cycles are not preserved in the stratigraphy of larger deltas, like the Ganges-Brahmaputra and Mississippi Deltas, due to their large autogenic space and time scales. Interestingly, the majority of systems explored lie close to the predicted storage thresholds, suggesting difficult to extract, but present stratigraphic signatures. We acknowledge some change in channel depths have occurred since the Late Miocene due to changing boundary conditions. These changes, though, are unlikely to influence our general result: autogenic processes likely make it difficult, if not impossible, to extract the stratigraphic signature of Milankovitch scale RSL fluctuations from medium to large deltaic deposits of greenhouse Earth conditions. This examination suggests a fundamental property of the stratigraphic record and its generation: that below critical thresholds autogenic and allogenic products cannot be separated due to a smearing of forcing conditions by the stratigraphic filter. This result is similar in spirit to

thresholds proposed in the routing of forcing conditions via fluid turbulence (von der Heydt et al., 2003) and sediment transport (Jerolmack and Paola, 2010).

While we performed several tests on the experimental physical stratigraphy, additional attributes of the stratigraphy can still be examined. However, to provide a rigorous test of RSL storage in stratigraphy, a test must include a comparison to a comparable system evolving in the absence of changing boundary conditions. As discussed previously (Van Wagoner et al., 1990; Dalman et al., 2015) autogenics, for example a cycle of channel extension, avulsion, abandonment, and later reoccupation, produce architecture with inherent scales which must be differentiated from allogenic product scales. This should also hold for analysis of trends in bio, chemo, and/or magneto-stratigraphy.

Further, our results emphasize the need to consider system dynamics in addition to geometry when developing stratigraphic theory. For example, while steep delta foresets are exposed during RSL fall in our shredded experiment, they do not result in incisional confinement greater than observed in our control experiment. Similar to theory proposed by Nijhuis et al. (2015), we suggest this occurs due to a slow morphodynamic response rate relative to the RSL fall rate.

While autogenic processes might limit the range of paleo-environmental information stored in stratigraphy, these thresholds can also be viewed in a positive light. Our results suggest strong statistical similarities between stratigraphy constructed solely by autogenic processes and stratigraphy constructed in the presence of shredded RSL cycles. Thus it might not be necessary for individuals performing

stratigraphic prediction to include these changing boundary conditions in forward deltaic evolution models. Simply modeling the internal dynamics should produce statistically reasonable predictions.

4.6 Summary

This study suggests quantitative limits to the fidelity of the stratigraphic record set by the space and time scales of autogenic processes. The thresholds proposed here likely limit our ability to invert this record for critical paleo-environmental information. While we focus on resolving paleo-RSL change in deltaic stratigraphy, similar stratigraphic thresholds, set by autogenic process scales, likely exist in other depositional environments and for other classes of signals (i.e. tectonics and upstream climatic forcings).

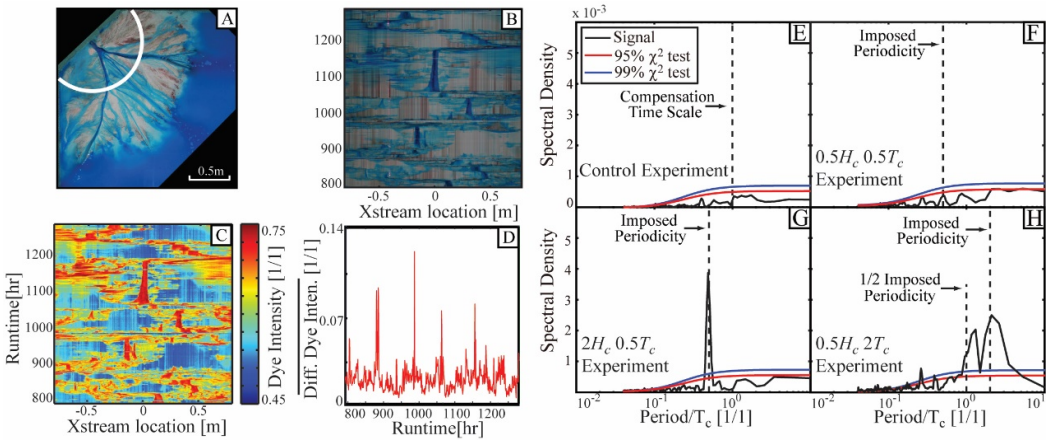

Figure 4.1 Analysis of surface morphodynamics along a proximal transect**.** Process involved in generating morphodynamic time series. (A) Photograph of the active delta top at run-hour 627. Solid white line represents transect defined by a 0.6 m radius from source. (B) RGB color values are extracted from images and compiled to generate time series of visible color along transect. (C) Matrix is converted to normalized dye intensity. (D) Time series of mean change in dye intensity between successive measurements generated and used as morphodynamic time series. E-H) Morphodynamic time series power spectra and χ^2 confidence limits.

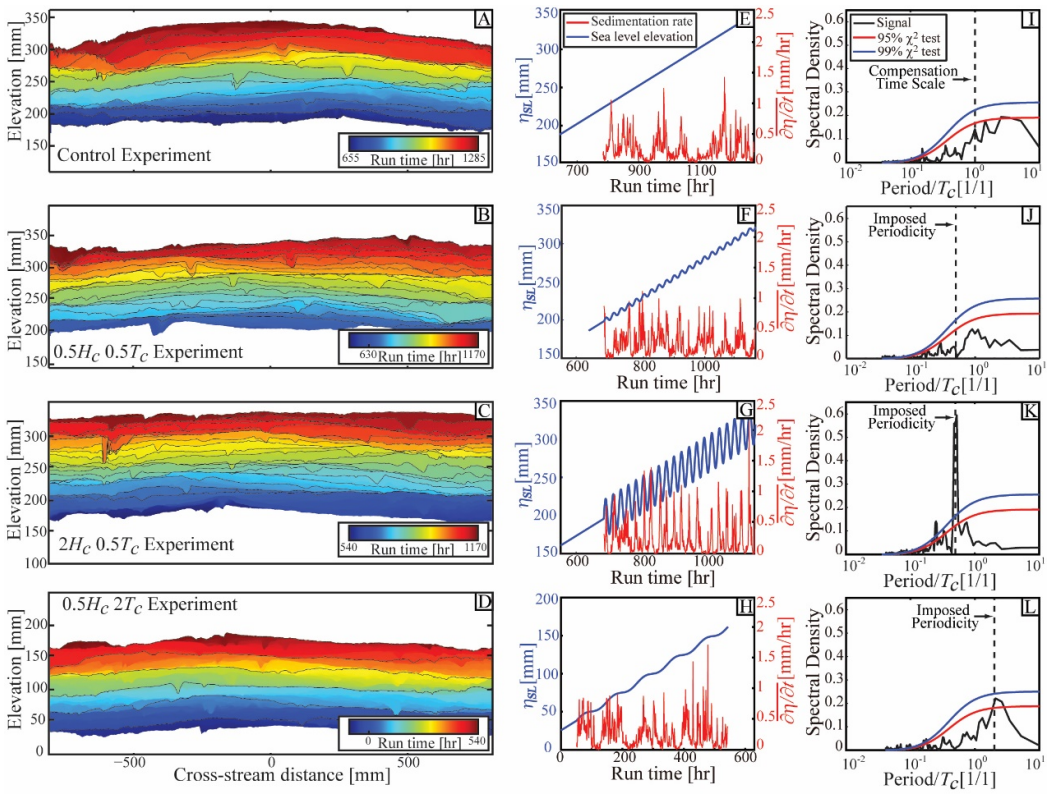

Figure 4.2 Analysis of mean deposition rate calculated from preserved experimental stratigraphy. A-D) Synthetic stratigraphy along a proximal transect with location illustrated in Figure 1A. Solid black lines represent time horizons separated by one T_c (A) or demarcating the start of each RSL cycle (B-D). E-H) Sea level (η_{SL}) and mean deposition rate time series; I-L) Power spectra of mean deposition rate time series and χ^2 confidence limits. Complimentary analysis performed at 1.1 m from source provided in Appendix to chapter 4.

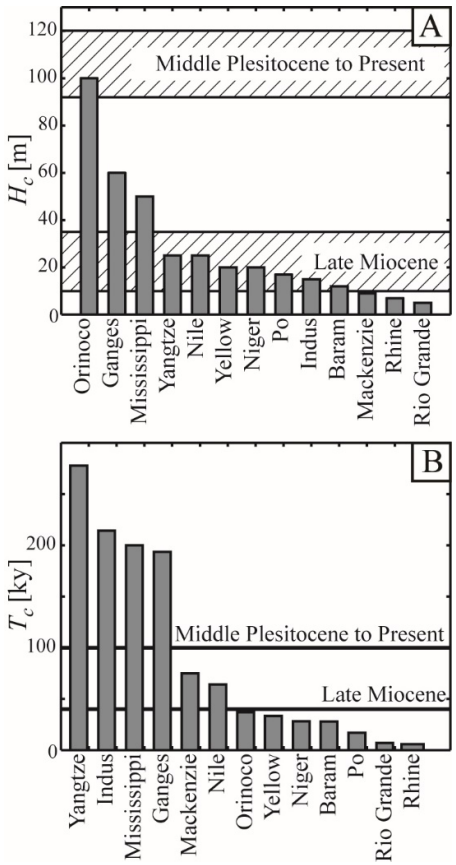

Figure 4.3 Comparison of autogenic spatial (A) and temporal (B) scales for major river systems to paleo-RSL cycle magnitudes and periodicities, respectively. Hashed regions in H_c compilation define range of Middle Pleistocene to Present and Late Miocene RSL cycles. Solid horizontal lines in T_c compilation define dominant Middle Pleistocene to Present eccentricity driven and dominant Late Miocene obliquity driven periodicity in sea level.

Appendix to chapter 4

A4.1 Additional Morphodynamic and Stratigraphic Analysis

In addition to the experiments discussed in the report body, two additional experiments were performed which were characterized by 1) $H^* = 1$, $T^* = 0.5$ and 2) $H^* = 4$, $T^* = 2$. Similar to the previously discussed experiments, these experiments shared the same input water and sediment feed rates and long term sea level rise rate. In each experiment, statistically significant peaks in spectral density were found at the time scale of imposed periodicity, indicating RSL signal storage (Figure S4.1). Analogous to modulated turbulence (von der Heydt et al., 2003) and shredding of sediment flux signals (Jerolmack and Paola, 2010), our results suggest that the threshold for signal shredding exists somewhere between 0.5 – 1.0 for both H^* and T^*.

Additional test were performed to search for the signature of RSL cycles in the stratigraphy and morphodynamics of experimental data sets. First, we perform an analysis of mean deposition rate time series for all experiments along a distal circular transect located at 1.1 m from the sediment and water source (Figure S4.2). This location approximates the mean spatial location of the shoreline in all experiments. Similar to our analysis of stratigraphic time series at 0.6 m from the source, we start by characterizing the power spectra of our control experiment. All power spectra in this study are generated with a MultiTaper Method (MTM) (Thomson, 1982). We produce confidence bands for the identification of statistically significant frequencies by performing a Chi-square test on the power spectra of our control experiment with a

red-noise model. For all confidence tests in this study, we assume an underlying autoregressive-1 “red noise” model, as in other studies which document correlation in morphodynamic (Jerolmack and Paola, 2010) and stratigraphic (Meyers, 2012) time series. These confidence bands are then used in analysis of the experiments with imposed RSL cycles. Similar to our analysis of the proximal transect, we find that statistically significant peaks are present at the periodicity of imposed RSL cycles in experiments with H^* and/or T^* values equal to or much greater than 1. However, no peak is observed in the experiment where H^* and T^* were much less than 1. Additionally, we find that the signal strength of all peaks is reduced along the distal, relative to proximal transect, suggesting optimal signal storage likely does not occur at the mean shoreline location.

To further search for the signature of the imposed RSL cycles in the preserved stratigraphy, we generate time series of the second moment of deposition rates measured along the two transects previously discussed. Specifically, we measure the standard deviation of deposition rates calculated for each pair of sequential time lines within the stratigraphy. This is similar in spirit, but not identical to, the regional stratigraphic variability time series analysis performed by Karamitopoulos et al. (2014). Similar to our time series analysis of mean deposition rates, we find significant peaks in spectra at the imposed RSL periodicity for experiments where T^* and/or H^* were greater than 1, while no statistically significant peak is observed in the spectra of the experiment where both T^* and H^* were less than 1. Results from the proximal transect are shown in figure S4.3.

Next, we compare aspects of the physical and synthetic stratigraphy of the four experiments. First, we compare the fraction of colored sand preserved in strike oriented cross-sections located 0.89 m from the basin inlet point (Figure S4.4A-E). The colored sand serves as a proxy for the coarse sand fraction input to the basin, as noted above. For each cross-section we calculated the fraction of the deposit composed of colored sand. Using a threshold color value, determined from visual inspection, we separated coarse colored sand deposits from fine white silica deposits. We implemented this technique using a range of plausible threshold values to assess error in our calculation. We find similar colored sand fractions preserved in the control and low H^* low T^* deposits, while the high T^* and high H^* deposits have significantly more preserved colored sand (Figure S4.4F). We also compared the dimensions of preserved channel bodies in the four experiments. Channel body widths and depths were measured along the same strike transect used for our proximal stratigraphic time series analysis. From this database we calculated 25%, 50%, and 75% channel body depths and width-to-depth ratios (Figure S4.4G-H). We observe significant differences in the channel body dimensions of our high H^* experiments from our control experiment, while the channel body dimensions of our two lower magnitude experiments are similar to our control experiment.

A4.2 Expanded Methods

The experiments performed in this study were conducted in the Delta Basin at Tulane University's Sediment Dynamics Laboratory. This basin is 2.8m wide by 4.2m

long and 0.65m deep. Accommodation is created in the Delta Basin by slowly increasing base level using a motorized weir that is in hydraulic communication with the basin. This system allows base-level control through a computer interface with submillimeter-scale resolution. Water and sediment supply to the basin are also controlled through the above-mentioned computer interface.

All experiments included an initial build out phase in which sediment and water were mixed in a funnel and fed from a single point source at the center of the upstream wall. After a system prograded ~1.1 m from the source to shoreline, the long term base-level rise was initiated at a rate equal to the total sediment discharge divided by the desired delta-top area. In each experiment, the combination of sediment feed rate and long term base-level rise allowed the shoreline to be maintained at an approximately constant location through the course of the experiment, with superimposed fluctuations associated with the imposed RSL cycles. Resulting deltas had topset slopes of ~$2x10^{-2}$ and foreset slops of ~$6x10^{-1}$ (Figure S4.5).

The experiments discussed in this manuscript are as follows:

TDB-12: Following progradation with no base level rise, the control experiment was run for 1285 hrs, the final 900 hrs with constant feeds of water and sediment.

TDB-14-1: Following progradation, this experiment aggraded for 140 hrs with no RSL cycles followed by 490 hrs of base level cycling defined by cycles with $R_{RSL} = 4H_c$ and $T_{RSL} = 2T_c$.

TDB-14-2: Following progradation, this experiment aggraded for 140 hrs with no

RSL cycles followed by 490 hrs of base level cycling defined by cycles with $R_{RSL} = 1H_c$ and $T_{RSL} = 0.5T_c$. This was then followed by aggradation for 50 hrs with no RSL cycles followed by 490 hrs of base level cycling defined by cycles with $R_{RSL} = 0.5H_c$ and $T_{RSL} = 0.5T_c$.

TDB-15-1: Following progradation, this experiment aggraded for 50 hrs with no RSL cycles followed by 490 hrs of base level cycling defined by cycles with $R_{RSL} = 0.5H_c$ and $T_{RSL} = 2T_c$. This was then followed by aggradation for 140 hrs with no RSL cycles followed by 490 hrs of base level cycling defined by cycles with $R_{RSL} = 2H_c$ and $T_{RSL} = 0.5T_c$.

The input sediment mixture was designed to mimic earlier experimental work (Hoyal and Sheets, 2009) and had a broad distribution, ranging from 1 – 1000 μm with a mean of 67 μm, and included a small amount of a polymer to enhance sediment cohesion. A fraction of the coarse tail of the distribution was replaced with dyed sediment of near equivalent grain size to aid visualization of stratigraphic architecture. In order to aid characterization of morphodynamics the input water was dyed with a food coloring.

Three types of data were collected from the experiments: system morphology, surface topography, and deposit stratigraphy. The morphologies of the fluvial systems were recorded with a digital camera positioned to collect images of the entire delta, which were used to characterize surface dynamics once every 15 min. Topography was monitored with a FARO Focus3D-S 120 laser scanner with a 5 mm horizontal grid in the down and cross basin directions, respectively. The vertical resolution of the

scanner is less than 1 mm. Topographic scans were collected once an hour for the duration of each experiment. This scanner also houses a digital camera, such that all topographic points are tagged with RGB color values, thus producing 3D photos. Each experimental stage produced an average of 120 mm of stratigraphy. Following each experiment, we sectioned and imaged the deposits along strike oriented transects 0.89 and 1.30 m from the basin infeed location.

A4.3 Experimental Parameters

H_c and T_c were defined through topographic analysis of the control experiment and were then used to define the magnitude and periodicity of RSL cycles in remaining three experiments (Table S4.1).

A4.4 Delta H_c & T_c database

Here we compile a data set of H_c and T_c estimates for field-scale basins using published data on river depths and long-term sedimentation rates, which includes 13 modern delta systems (Table S4.2 and Figure S4.6). Our data set only utilizes sedimentation rates measured for time intervals in excess of 100 kyrs. As shown by Sadler (1981), for a wide range of time scales, sedimentation rate is a function of the interval of measurement. However, Jerolmack and Sadler (2007) showed that persistence in deposition rates as a function of measurement interval is reached at time scales in excess of 100 kyr for deltas.

Experiment	H_c [mm]	T_c [hr]
Control	12.5	49

	R_{RSL}	T_{RSL}
0.5 H_c 0.5 T_c	6.25	24.5
0.5 H_c 2 T_c	6.25	98
2 H_c 0.5 T_c	25	24.5
1 H_c 0.5 T_c	12.5	24.5
4 H_c 2 T_c	50	98

Table S4.1 Autogenic limits and RSL attributes for physical experiments.

System	*Hc* [m]	$\bar{r}$ [mm/yr]	*Tc* [kyr]
1) Orinoco - eastern Venezuela	100	2.7	371
2) Ganges - India	60	0.31	194
3) Mississippi - Southern USA	50	0.25	200
4) Yangtze - Eastern China	25	0.09	278
5) Nile - Northern Egypt	25	0.39	64
6) Yellow - Eastern China	20	0.6	33
7) Niger - Nigeria	20	0.71	28
8) Po - Northern Italy	17	1	17
9) Indus - Pakistan	15	0.07	214
10) Baram - Malaysia	12	0.43	28
11) Mackenzie - Northwest Canada	9	0.12	75
12) Rhine - The Netherlands	7	1.2	6
13) Rio Grande - Southwestern USA	5	0.71	7

Table S4.2 Compilation of parameters controlling autogenic space and time scales for field scale systems (Oomkens, 1974; Zagwijn, 1989; El‐Ella, 1990; LINDSAY et al., 1991; Chukwueke et al., 1992; Chen and Stanley, 1995; Sandal, 1996; Wang and Evans, 1997; Allison, 1998; Wood, 2000; Hill et al., 2001; Carminati and Martinelli, 2002; Clift et al., 2002; Saller, 2003; Banfield, 2004; Inam et al., 2007; Cui et al., 2008; Nittrouer et al., 2008; Hijma et al., 2009; Straub et al., 2009; Said, 2013; Wang and Andutta, 2013).

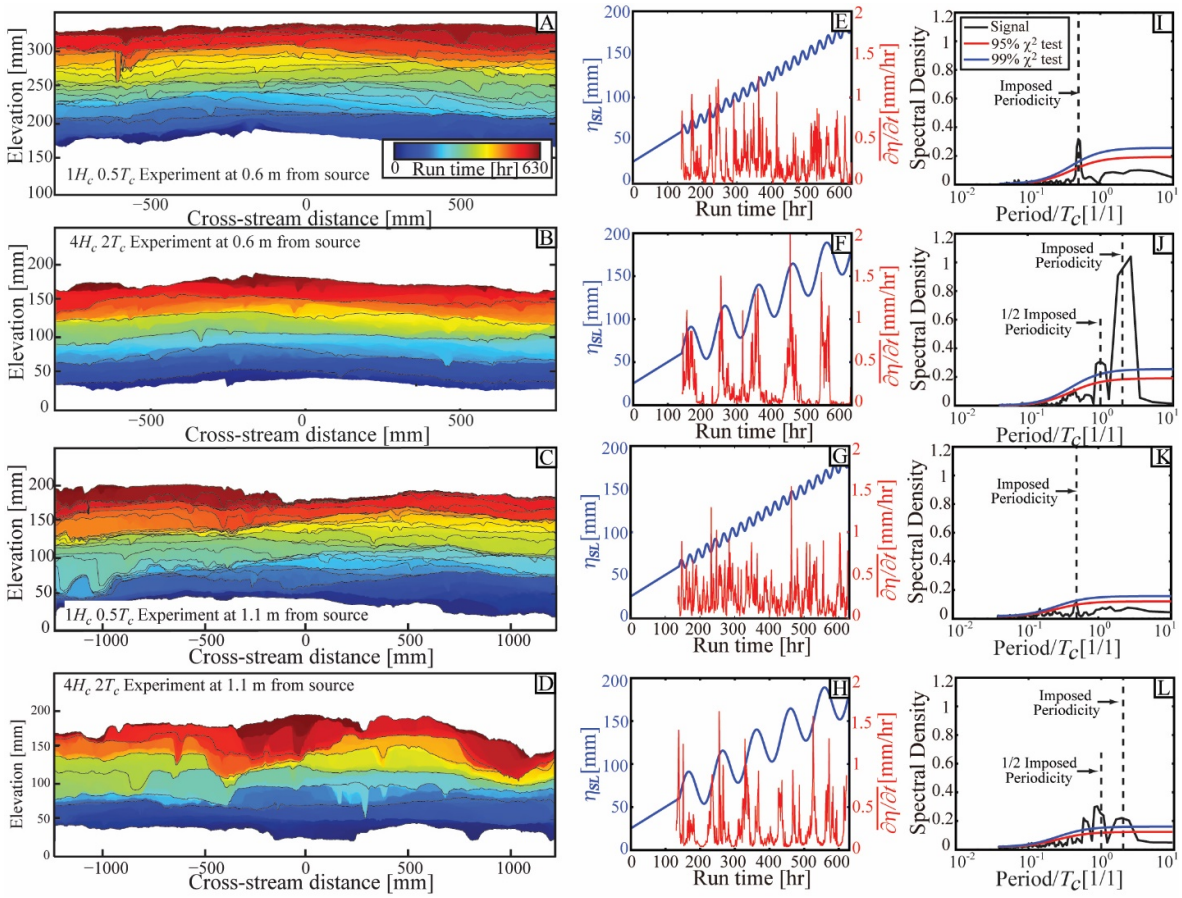

Figure S4.1 Time series analysis of mean deposition rate calculated from preserved stratigraphy for additional experiments not discussed in main report text with comparison to sea level time series. A-D) Synthetic stratigraphy along proximal (0.6 m radius from source) and distal (1.1 m radius from source) transects. Solid black lines represent time horizons separated by 1 T_c (A) or demarcating the start of each RSL cycle (B-D). E-H) Sea level and mean deposition rate time series along distal transects; I-L) Power spectra of mean deposition rate time series and χ^2 confidence limits.

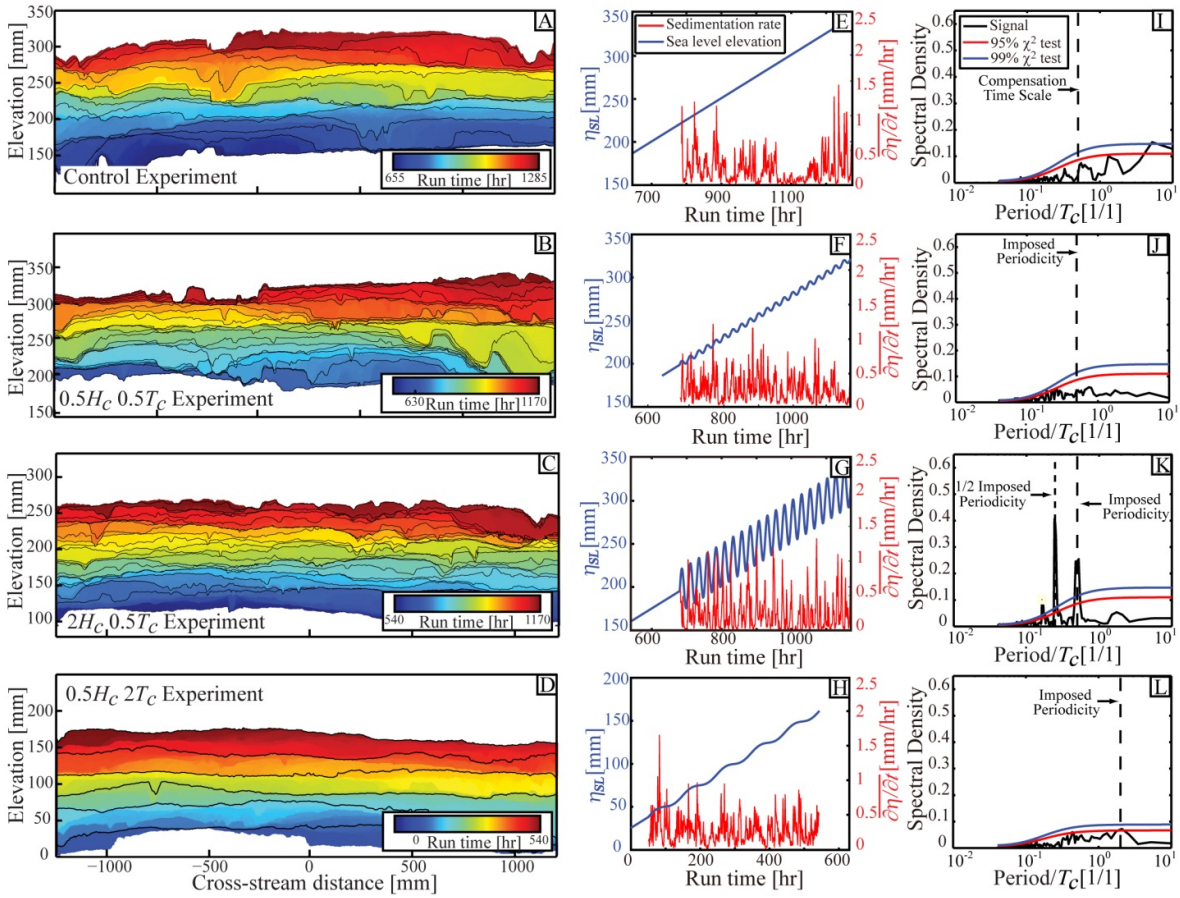

Figure S4.2 Time series analysis of mean deposition rate calculated from preserved distal stratigraphy for all experimental deltas with comparison to sea level time series. A-D) Synthetic stratigraphy along a distal transect defined by a 1.1 m radius from source. Solid black lines represent time horizons separated by 1 T_c (A) or demarcating the start of each RSL cycle (B-D). E-H) Sea level and mean deposition rate time series along distal transects; I-L) Power spectra of mean deposition rate time series and χ^2 confidence limits.

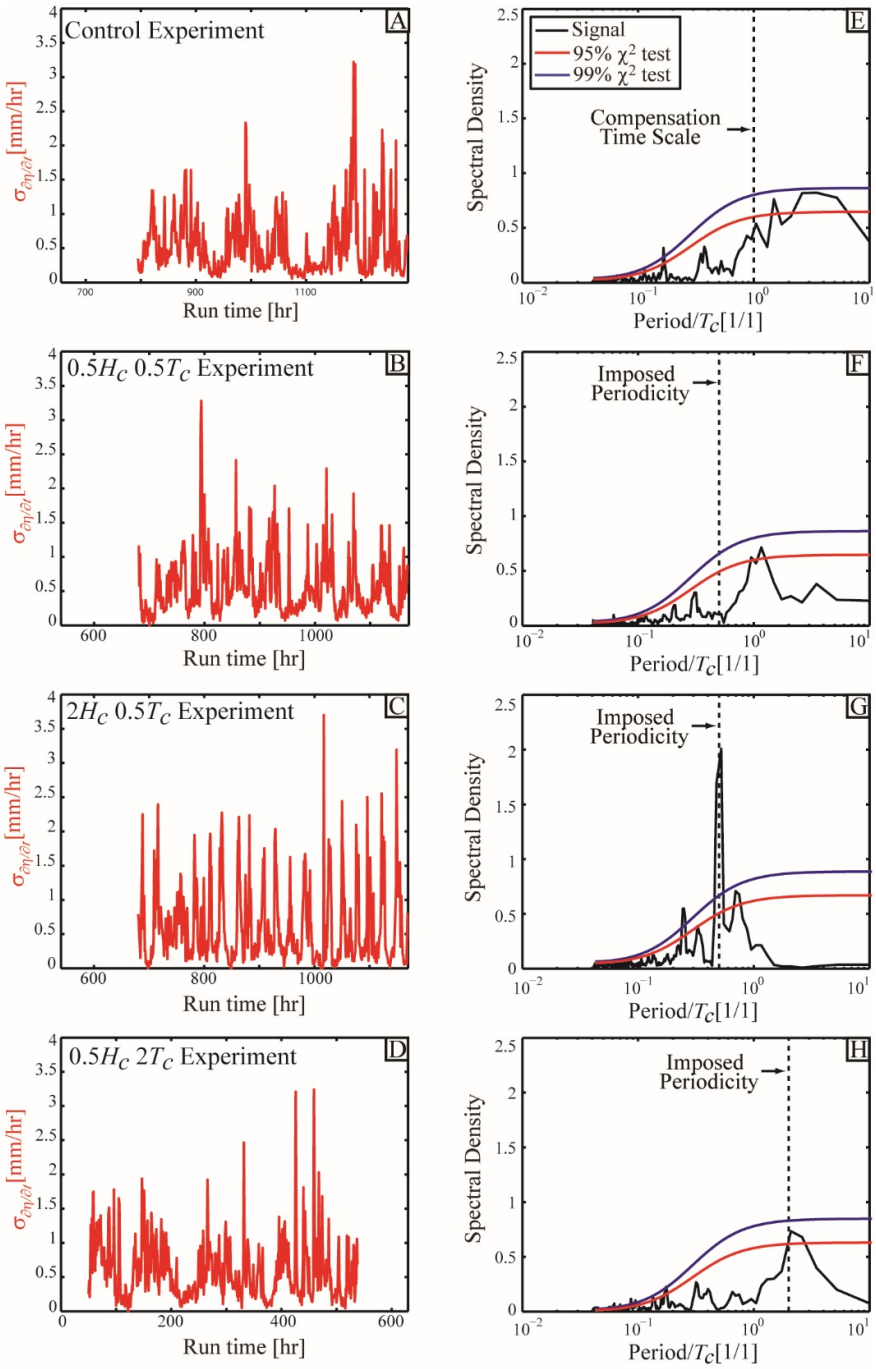

Figure S4.3 Time series analysis of the standard deviation of deposition rate calculated from preserved proximal stratigraphy for all experimental deltas. A-D) Standard deviation of deposition rate time series along proximal transects; I-L) Power spectra of mean deposition rate time series and χ^2 confidence limits.

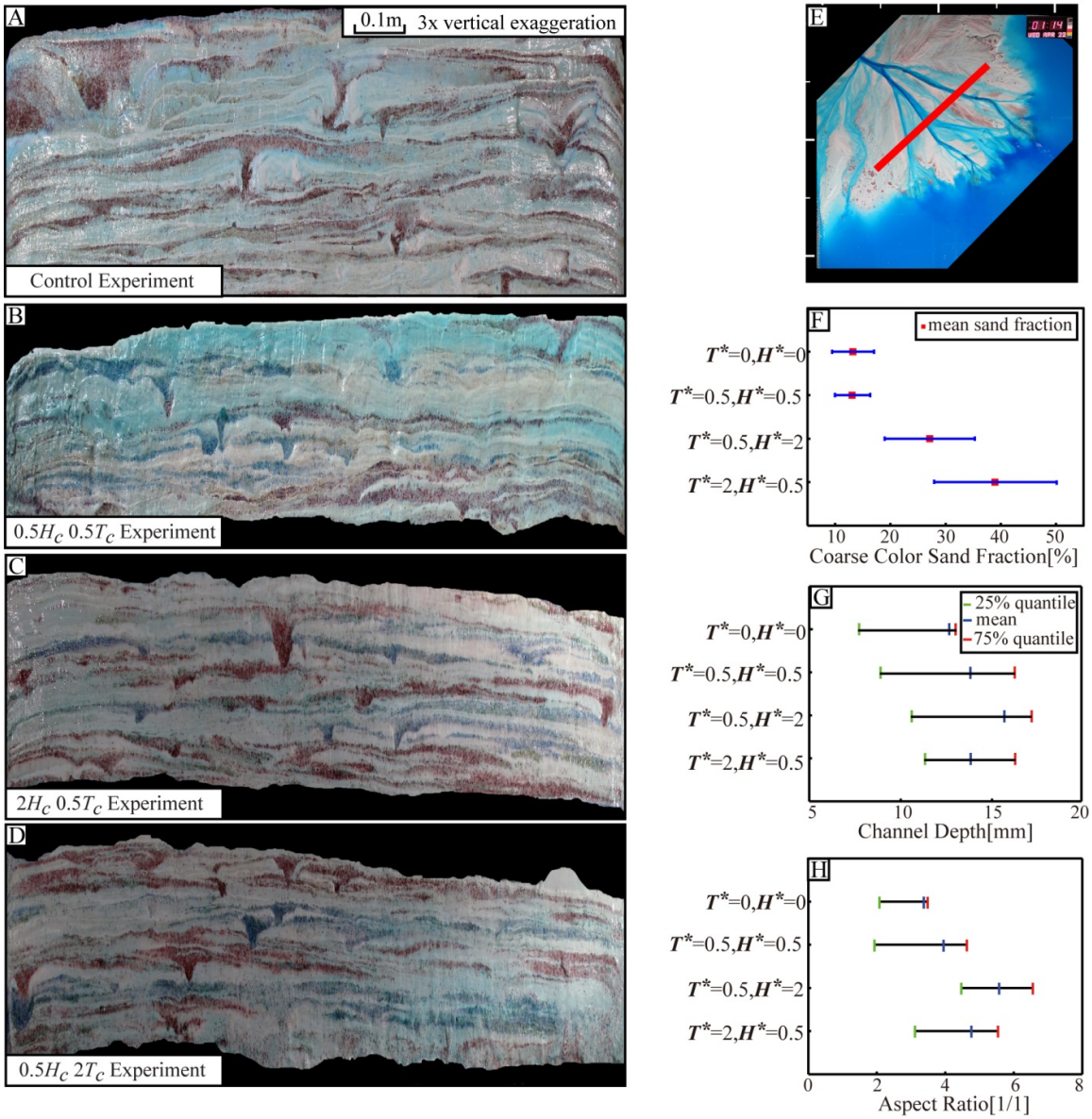

Figure S4.4 Comparison of physical stratigraphy in four experiments. A-D) Images of physical stratigraphy displayed as if looking from source to sink. E) Overhead image of active experiment with location of stratigraphic panels shown with solid red line. F) Comparison of coarse color sand fraction in physical stratigraphic panels from each experiment. Error bars represent range of coarse colored sand fraction estimated from the range of threshold color values used to separate colored sand deposits from fine white deposits. G) Comparison of mean and range of channel depths, where range is expressed by the 1st and 3rd quartile. H) Comparison of mean and range of channel width-to-depth ratio in experiments.

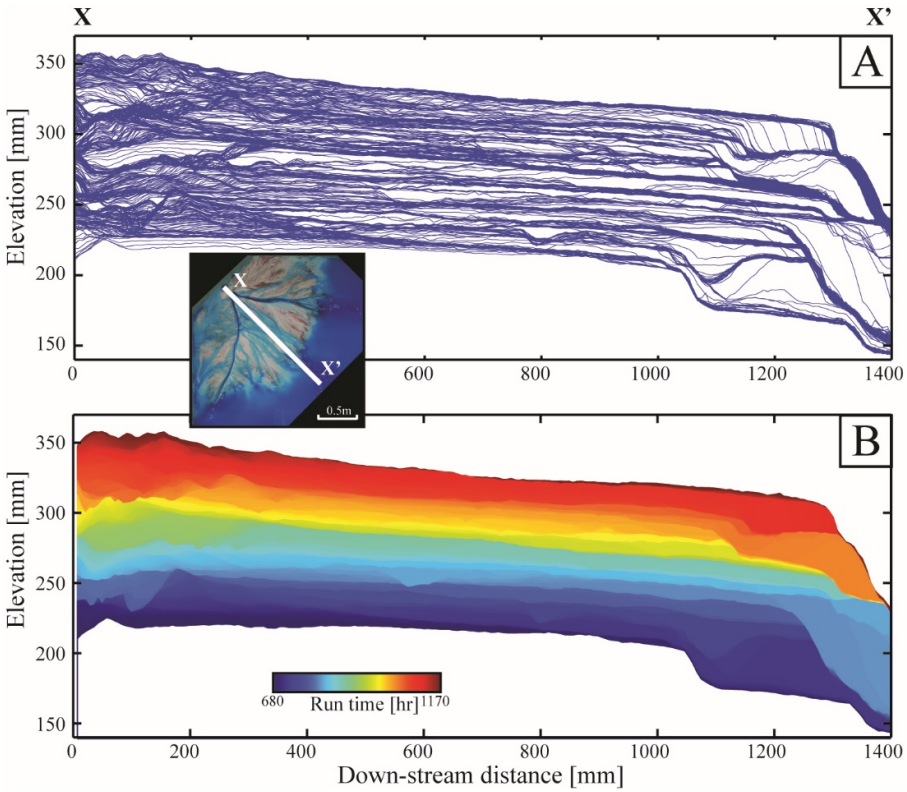

Figure S4.5 Synthetic stratigraphy along a dip transect initiating at the basin entrance and extending 1400 mm in the distal direction (X – X'). A) Synthetic stratigraphy generated from stacked topographic transects clipped for erosion. B) Synthetic stratigraphy with color defining time of sediment deposition.

Figure S4.6 Location map of river deltas used in compilation of field scale systems. Red dots give locations of deltas used in compilation. Numbers correspond to deltas listed in Table 4S.2.

Chapter 5

Conclusions

This thesis is broadly centered on the theme of discriminating autogenic from allogenic processes and stratigraphic products along source to sink sediment paths. In erosional landscapes, I characterized how different temporal patterns of rock uplift change influence sediment flux signals at the outlet of erosional landscapes. In the sedimentary system, I measured how sediment cohesion influences the temporal and spatial scales of autogenic processes and how surface dynamics translate into stratigraphy. In addition, I defined storage thresholds for relative sea level cycles in stratigraphy. Results from this thesis highlight that the magnitude and time scale of both autogenic and allogenic processes control how signals propagate through landscapes and if these signals are stored in stratigraphy. In addition, theory and observations from this thesis advance our capacity to differentiate the products of autogenic and allogenic processes, thus improving our ability to invert surface processes and stratigraphic records for paleo-environmental signals.

In chapter two, I performed a series of numerical experiments under different temporal patterns of rock uplift rate. Due to the non-linear response of sediment flux to changes in rock uplift rate, I observed that sediment flux can increase even if rock uplift rate is decreasing. One could further use the landscape morphology (Kirby and Whipple, 2012) and characteristics of sediment flux to accurately judge whether rock uplift rate has most recently increased or decreased. The time lag between changes in

rock uplift rate and a response in the sediment flux also determines whether a rock uplift signal will be evident in a sediment flux signal. Specifically, I find that relatively short duration changes in rock uplift rate may not translate into a sediment flux signal, even in models that lack stochastic autogenic processes.

Results from our modeling of erosional landscapes also suggest that time series of sediment flux have the greatest potential to illustrate the magnitude of rock uplift changes if the duration of high and low uplift rates are both at least equal to or greater than response time of the landscape. Our results, when combined with previous studies (Whipple and Tucker, 1999; Whipple, 2001), suggest that the response time of a landscape to a perturbation in rock uplift rate is mainly associated with the drainage area and erodibility of a watershed. Systems with small drainage areas will have shorter landscape response times, all else being equal. As a result, we might expect better preservation of rock uplift changes in field systems with small drainage areas, such as the Golo catchment in Eastern Corsica (A ~1,000 km^2) (Calves et al., 2013). However, a landscape near a convergent boundary with a large drainage area, such as the Arun Valley in Himalayan orogen (A ~ 58,000 km^2) (Olen et al., 2015), is less likely to preserve complete records of rock uplift changes due to long system response times.

While drainage area is relatively straight forward to measure, I note that in field settings it can be difficult to directly measure the erodibility of a landscape, which is necessary to constrain landscape response time (Murray et al., 2016) . However, we know that high erodibility often corresponds to field settings where bedrock has a

weak lithological composition in wet climates. As such, we might expect a system in a tropical region, such as the Amazon drainage system, to better preserve rock uplift signals compared to a system with a similar drainage area in a drier region.

If changes in rock uplift result in sediment flux signals, a characteristic stratigraphic pattern might be expected in downstream depositional basins. For example, numerical models performed by Armitage et al. (2011) show that changes in rock uplift rate produce characteristic responses in the caliber of sediment delivered to depositional basins. Changes to the size of sediment delivered to deltaic depocenters could influence sediment cohesivity (Edmonds and Slingerland, 2010; Caldwell and Edmonds, 2014). In chapter three, we use physical experiments to explore how sediment cohesion influences critical deltaic autogenic time and space scales. We show that sediment cohesion promotes the development of deep and stable channels. This enhaced channelization reduces the lateral mobility of cohesive systems. As a result, an increase in sediment cohesion increases the temporal and spatial scales of autogenic transgressions and regressions. In addition, I utilzed topographic data and channel maps to estimate the time scales of system mobility associated with topograhic modification, and a time scale of channel mobiliy only related to topographic changes caused by channels. While sediment cohesion increases the time scale of lateral mobility, both for the whole system and the channels, the lateral mobility of the channels decreases more than the decrease in total system mobility. This result suggests that an increase in sediment cohesion increases the pumping of suspended sediment to overbank environments. Furthermore, I find that sediment

cohesion increases depositional persistence. As a result, the variability in sedimentation patterns, relative to the spatial pattern of accomodation generation, increases. The enhanced depositional persistence is also linked to segregation of fine overbank sediments from coarse channel and lobe deposits.

A critical autogenic length scale highlighted in this thesis and in several recently published studies is the maximum depth of a system's channels (Wang et al., 2011; Straub and Wang, 2013). Channel depth has previously been linked to the ratio of water to sediment flux in a channel (Parker, 2004). As such, channel depth can be influenced both by the rate of rock uplift in an erosional landscape which could change sediment flux (chapter 2) and the sediment cohesion in a system (chapter 3). In chapter 4, I use this autogenic length scale and an autogenic time scale, T_c, to define the conditions necessary to store signals of relative sea level in deltaic stratigraphic records. Specifically, using overhead images and topographic data, we generate time series of key morphodynamic and stratigraphic variables. Power spectral analyses of these time series show that the extraction of RSL cycles from the physical stratigraphic record requires their magnitudes and periodicities to be greater than the spatial and temporal scales of the autogenic dynamics of deltas.

To explore the possible influence of stratigraphic signal shredding on Milankovic scale RSL cycles, I compiled a database of channel depths and compensation time scales for medium to large deltaic depocenters. I observe that large magnitude and long periodicity RSL cycles during icehouse (Pleistocene to present) Earth conditions should be preserved in the vast majority of deltaic system. However, small magnitude

and short periodicity RSL cycles during proxy greenhouse (Late Miocene) Earth conditions have high shredding potential in large systems like the Mississippi and Ganges River Deltas.

Interestingly, both the Mississippi and Ganges deltaic depocenters are covered by dense vegetation that increases their cohesivity. This likely enhances their channel depths, thus increasing their autogenic space and time scales compared to less cohesive systems like the Yellow River Delta (Edmonds and Slingerland, 2010). Taken together, results from chapters 3 and 4 suggest that the optimal conditions for storing relative sea level signals include systems with shallow channels, resulting from either low sediment cohesion and/or low ratios of water to sediment flux, and basins with high long term subsidence rates.

Finally, I close by noting that chapter 4 provides a framework for predicting the attributes that environmental signals need to posses, relative to a system's internal dynamics, for storage in the stratigraphic record. This theory is developed for the storage of relative sea level signals, but can likely be augmented to define storage thresholds for other classes of environmental signals, such as sediment flux cycles produced by changing rock uplift rates.

Appendix Datasets

In this thesis, I conducted ten numerical experiments and five physical experiments, generating approximately 6 TB datasets.

In chapter two, I used the CHILD model to conduct numerical experiments. This model can be download from the Community Surface Dynamics Modeling System at: https://csdms.colorado.edu/wiki/Model:CHILD

Data resulting from the physical experimental has been uploaded to the Sustainable Environment – Actionable Data (SEAD) project data repository in collaboration with the Sediment Experimentalist Network (SEN). Data can be found in the folder for the Tulane Sediment Dynamics and Stratigraphy (TSDS) group under the Collections menu. The link is: https://sen.ncsa.illinois.edu/acr/#collection?uri=tag:cet.ncsa.uiuc.edu,2008:/bean/Collection/5A2390DB-5C8E-4393-BEE1-C7C3D2DEF644.

Data from the weakly and moderately cohesive experimental stages discussed in chapter two, can be found under the folder named TDB_13_1. Data from the strongly cohesive experimental stage can be found under the folder named TDB_12_1. Data from the 4th chapter associated with the experiment where $T^*= 2$ & $H^*= 4$ can be found under the folder named TDB_14_1. Data from the experimental stages where $T^*= 0.5$ & $H^*= 1$ and or $T^*= 0.5$ & $H^*=0.5$ can be found under the folder named TDB_14_2. In each dataset folder, one can find experimental logs, original/raw data sets and processed results. In this thesis, I mainly use topographic scans that are taken during pauses of the experiments to calculate a suite of metrics, including a

compensation index and time series of sedimentation rates. Using TDB_13_1 as an example, you can locate these dry scans by following the directory, TDB_13_1\ TDB_13_1Results and Processed Data \TDB_13_1_Topo_Data \ Matrix_Form \ TDB_13_1_Dry_Z.

Digital images of the physical stratigraphy which have been used to quantify the segregation of fine from coarse materials in the stratigraphic sections are also available. You can locate these digital images by following the directory, TDB_13_1\TDB_13_1 Original Data\Subside\Cuts. If you meet any problems in accessing the data sets that have been used in this thesis, please feel to contact me through the email: qli1@tulane.edu.

Reference

Ahnert, F., 1970, Functional relationships between denudation, relief, and uplift in large, mid-latitude drainage basins: American Journal of Science, v. 268, no. 3, p. 243-263.

Allen, P. A., 2008, From landscapes into geological history: Nature, v. 451, no. 7176, p. 274-276.

Allison, M. A., 1998, Historical changes in the Ganges-Brahmaputra delta front: Journal of Coastal Research, p. 1269-1275.

Armitage, J. J., Duller, R. A., Whittaker, A. C., and Allen, P. A., 2011, Transformation of tectonic and climatic signals from source to sedimentary archive: Nature Geoscience, v. 4, no. 4, p. 231-235.

Armitage, J. J., Jones, T. D., Duller, R. A., Whittaker, A. C., and Allen, P. A., 2013, Temporal buffering of climate-driven sediment flux cycles by transient catchment response: Earth and Planetary Science Letters, v. 369, p. 200-210.

Aslan, A., and Blum, M., 1999, Contrasting styles of Holocene avulsion, Texas Gulf coastal plain, USA: Fluvial sedimentology VI, p. 193-209.

Banfield, L. A., 2004, Late Quaternary evolution of the Rio Grande delta: complex response to eustasy and climate change.

Beerbower, J. R., 1961, Origin of cyclothems of the Dunkard group (upper Pennsylvanian-lower Permian) in Pennsylvania, West Virginia, and Ohio: Geological Society of America Bulletin, v. 72, no. 7, p. 1029-1050.

-, Cyclothems and cyclic depositional mechanisms in alluvial plain sedimentation, *in* Proceedings Symposium on Cyclic Sedimentation: State Geological Survey of Kansas, Bulletin1964, Volume 169, p. 31-42.

Blum, M. D., and Törnqvist, T. E., 2000, Fluvial responses to climate and sea‐level change: a review and look forward: Sedimentology, v. 47, no. s1, p. 2-48.

Braudrick, C. A., Dietrich, W. E., Leverich, G. T., and Sklar, L. S., 2009, Experimental evidence for the conditions necessary to sustain meandering in coarse-bedded rivers: Proceedings of the National Academy of Sciences, v. 106, no. 40, p. 16936-16941.

Buehler, H. A., Weissmann, G. S., Scuderi, L. A., and Hartley, A. J., 2011, Spatial and temporal evolution of an avulsion on the Taquari River distributive fluvial system from satellite image analysis: Journal of Sedimentary Research, v. 81, no. 8, p. 630-640.

Burpee, A. P., Slingerland, R. L., Edmonds, D. A., Parsons, D., Best, J., Cederberg, J., McGuffin, A., Caldwell, R., Nijhuis, A., and Royce, J., 2015, Grain-Size Controls On the Morphology and Internal Geometry of River-Dominated Deltas: Journal of Sedimentary Research, v. 85, no. 6, p. 699-714.

Caldwell, R. L., and Edmonds, D. A., 2014, The effects of sediment properties on deltaic processes and morphologies: A numerical modeling study: Journal of Geophysical Research: Earth Surface, v. 119, no. 5, p. 961-982.

Calves, G., Toucanne, S., Jouet, G., Charrier, S., Thereau, E., Etoubleau, J., Marsset, T., Droz, L., Bez, M., and Abreu, V., 2013, Inferring denudation variations

from the sediment record; an example of the last glacial cycle record of the Golo Basin and watershed, East Corsica, western Mediterranean sea: Basin Research, v. 25, no. 2, p. 197-218.

Carminati, E., and Martinelli, G., 2002, Subsidence rates in the Po Plain, northern Italy: the relative impact of natural and anthropogenic causation: Engineering Geology, v. 66, no. 3, p. 241-255.

Cazanacli, D., Paola, C., and Parker, G., 2002, Experimental steep, braided flow: application to flooding risk on fans: Journal of Hydraulic Engineering, v. 128, no. 3, p. 322-330.

Chen, Z., and Stanley, D. J., 1995, Quaternary subsidence and river channel migration in the Yangtze delta plain, eastern China: Journal of Coastal Research, p. 927-945.

Chukwueke, C., Thomas, G., and Delfaud, J., 1992, Processus sédimentaires, eustatisme, subsidence et flux thermique dans la partie distale du Delta du Niger: Bulletin des Centres de Recherches et Exploration-Production de Elf Aquitaine, v. 16.

Clift, P., Gaedicke, C., Edwards, R., Lee, J. I., Hildebrand, P., Amjad, S., White, R. S., and Schlüter, H.-U., 2002, The stratigraphic evolution of the Indus Fan and the history of sedimentation in the Arabian Sea: Marine Geophysical Researches, v. 23, no. 3, p. 223-245.

Cui, S., Liu, H., Tong, S., Zhang, J., Wu, Z., and Wu, J., 2008, Seismic stratigraphy of the quaternary Yellow River delta, Bohai Sea, eastern China: Marine Geophysical Researches, v. 29, no. 1, p. 27-42.

Dalman, R., Weltje, G. J., and Karamitopoulos, P., 2015, High-resolution sequence stratigraphy of fluvio–deltaic systems: Prospects of system-wide chronostratigraphic correlation: Earth and Planetary Science Letters, v. 412, p. 10-17.

Davies, N. S., and Gibling, M. R., 2010, Cambrian to Devonian evolution of alluvial systems: the sedimentological impact of the earliest land plants: Earth-Science Reviews, v. 98, no. 3, p. 171-200.

-, 2011, Evolution of fixed-channel alluvial plains in response to Carboniferous vegetation: Nature Geoscience, v. 4, no. 9, p. 629-633.

Edmonds, D. A., Hajek, E. A., Downton, N., and Bryk, A. B., 2016, Avulsion flow-path selection on rivers in foreland basins: Geology, p. G38082. 38081.

Edmonds, D. A., and Slingerland, R. L., 2010, Significant effect of sediment cohesion on delta morphology: Nature Geoscience, v. 3, no. 2, p. 105-109.

El‐Ella, R. A., 1990, THE NEOGENE‐QUATERNARY SECTION IN THE NILE DELTA, EGYPT: GEOLOGY AND HYDROCARBON POTENTIAL: Journal of Petroleum Geology, v. 13, no. 3, p. 329-340.

Forzoni, A., Storms, J. E., Whittaker, A. C., and Jager, G., 2014, Delayed delivery from the sediment factory: modeling the impact of catchment response time to tectonics on sediment flux and fluvio‐deltaic stratigraphy: Earth Surface Processes and Landforms, v. 39, no. 5, p. 689-704.

Galloway, W. E., 1975, Process framework for describing the morphologic and

stratigraphic evolution of deltaic depositional systems.

Gibling, M. R., 2006, Width and thickness of fluvial channel bodies and valley fills in the geological record: a literature compilation and classification: Journal of sedimentary Research, v. 76, no. 5, p. 731-770.

Gilbert, G. K., 1890, Lake Bonneville, US Government Printing Office.

Grabowski, R. C., Droppo, I. G., and Wharton, G., 2011, Erodibility of cohesive sediment: the importance of sediment properties: Earth-Science Reviews, v. 105, no. 3, p. 101-120.

Gust, G., and Müller, V., 1997, Interfacial hydrodynamics and entrainment functions of currently used erosion devices: Cohesive sediments, p. 149-174.

Hack, J. T., 1957, Studies of longitudinal stream profiles in Virginia and Maryland, 2330-7102.

Hajek, E. A., Heller, P. L., and Sheets, B. A., 2010, Significance of channel-belt clustering in alluvial basins: Geology, v. 38, no. 6, p. 535-538.

Heller, P. L., Paola, C., Hwang, I.-G., John, B., and Steel, R., 2001, Geomorphology and sequence stratigraphy due to slow and rapid base-level changes in an experimental subsiding basin (XES 96-1): AAPG bulletin, v. 85, no. 5, p. 0817-0838.

Hicks, D. M., Duncan, M. J., Walsh, J. M., Westaway, R. M., and Lane, S. N., 2002, New views of the morphodynamics of large braided rivers from high-resolution topographic surveys and time-lapse video: IAHS PUBLICATION, p. 373-380.

Hijma, M. P., Cohen, K., Hoffmann, G., Van der Spek, A. J., and Stouthamer, E., 2009, From river valley to estuary: the evolution of the Rhine mouth in the early to middle Holocene (western Netherlands, Rhine-Meuse delta): Netherlands journal of geosciences, v. 88, no. 01, p. 13-53.

Hill, P. R., Lewis, C. P., Desmarais, S., Kauppaymuthoo, V., and Rais, H., 2001, The Mackenzie Delta: Sedimentary processes and facies of a high‐latitude, fine‐grained delta: Sedimentology, v. 48, no. 5, p. 1047-1078.

Hooke, R. L., 1968, Model geology: prototype and laboratory streams: discussion: Geological Society of America Bulletin, v. 79, no. 3, p. 391-394.

Hoyal, D., and Sheets, B., 2009, Morphodynamic evolution of experimental cohesive deltas: Journal of Geophysical Research: Earth Surface (2003–2012), v. 114, no. F2.

Hutton, J., 1788, X. Theory of the Earth; or an Investigation of the Laws observable in the Composition, Dissolution, and Restoration of Land upon the Globe: Transactions of the Royal Society of Edinburgh, v. 1, no. 02, p. 209-304.

Inam, A., Clift, P. D., Giosan, L., Tabrez, A. R., Tahir, M., Rabbani, M. M., and Danish, M., 2007, The geographic, geological and oceanographic setting of the Indus River: Large rivers: geomorphology and management, p. 333-345.

Jerolmack, D. J., and Mohrig, D., 2007, Conditions for branching in depositional rivers: Geology, v. 35, no. 5, p. 463-466.

Jerolmack, D. J., and Paola, C., 2010, Shredding of environmental signals by sediment transport: Geophysical Research Letters, v. 37, no. 19.

Jerolmack, D. J., and Sadler, P., 2007, Transience and persistence in the depositional record of continental margins: Journal of Geophysical Research: Earth Surface, v. 112, no. F3.

Karamitopoulos, P., Weltje, G. J., and Dalman, R., 2014, Allogenic controls on autogenic variability in fluvio‐deltaic systems: inferences from analysis of synthetic stratigraphy: Basin Research, v. 26, no. 6, p. 767-779.

Kim, W., and Jerolmack, D. J., 2008, The pulse of calm fan deltas: The Journal of Geology, v. 116, no. 4, p. 315-330.

Kim, W., and Paola, C., 2007, Long-period cyclic sedimentation with constant tectonic forcing in an experimental relay ramp: Geology, v. 35, no. 4, p. 331-334.

Kim, W., Sheets, B. A., and Paola, C., 2010, Steering of experimental channels by lateral basin tilting: Basin Research, v. 22, no. 3, p. 286-301.

Kirby, E., and Whipple, K. X., 2012, Expression of active tectonics in erosional landscapes: Journal of Structural Geology, v. 44, p. 54-75.

Kleinhans, M. G., van Dijk, W. M., van de Lageweg, W. I., Hoyal, D. C., Markies, H., van Maarseveen, M., Roosendaal, C., van Weesep, W., van Breemen, D., and Hoendervoogt, R., 2014, Quantifiable effectiveness of experimental scaling of river-and delta morphodynamics and stratigraphy: Earth-Science Reviews, v. 133, p. 43-61.

LINDSAY, J. F., HOLLIDAY, D. W., and HULBERT, A. G., 1991, Sequence Stratigraphy and the Evolution of the Ganges-Brahmaputra Delta Complex (1): AAPG Bulletin, v. 75, no. 7, p. 1233-1254.

Martin, J., Sheets, B., Paola, C., and Hoyal, D., 2009, Influence of steady base‐level rise on channel mobility, shoreline migration, and scaling properties of a cohesive experimental delta: Journal of Geophysical Research: Earth Surface (2003–2012), v. 114, no. F3.

Meigs, A. J., Cooke, M. L., and Marshall, S. T., 2008, Using vertical rock uplift patterns to constrain the three-dimensional fault configuration in the los angeles basin: Bulletin of the Seismological Society of America, v. 98, no. 1, p. 106-123.

Meyers, S. R., 2012, Seeing red in cyclic stratigraphy: Spectral noise estimation for astrochronology: Paleoceanography, v. 27, no. 3.

Miller, K. G., Kominz, M. A., Browning, J. V., Wright, J. D., Mountain, G. S., Katz, M. E., Sugarman, P. J., Cramer, B. S., Christie-Blick, N., and Pekar, S. F., 2005, The Phanerozoic record of global sea-level change: science, v. 310, no. 5752, p. 1293-1298.

Murray, A. B., Gasparini, N. M., Goldstein, E. B., and Wegen, M. v. d., 2016, Uncertainty quantification in modeling earth surface processes: more applicable for some types of models than for others: Computer&Geosciences.

Murray, A. B., and Paola, C., 2003, Modelling the effect of vegetation on channel pattern in bedload rivers: Earth Surface Processes and Landforms, v. 28, no. 2, p. 131-143.

Muto, T., and Steel, R. J., 2004, Autogenic response of fluvial deltas to steady

sea-level fall: Implications from flume-tank experiments: Geology, v. 32, no. 5, p. 401-404.

Nardin, W., and Edmonds, D. A., 2014, Optimum vegetation height and density for inorganic sedimentation in deltaic marshes: Nature Geoscience, v. 7, no. 10, p. 722-726.

Nijhuis, A., Edmonds, D., Caldwell, R., Cederberg, J., Slingerland, R., Best, J., Parsons, D., and Robinson, R., 2015, Fluvio-deltaic avulsions during relative sea-level fall: Geology, v. 43, no. 8, p. 719-722.

Nittrouer, J. A., Allison, M. A., and Campanella, R., 2008, Bedform transport rates for the lowermost Mississippi River: Journal of Geophysical Research: Earth Surface, v. 113, no. F3.

Olen, S. M., Bookhagen, B., Hoffmann, B., Sachse, D., Adhikari, D., and Strecker, M. R., 2015, Understanding erosion rates in the Himalayan orogen: A case study from the Arun Valley: Journal of Geophysical Research: Earth Surface, v. 120, no. 10, p. 2080-2102.

Oomkens, E., 1974, Lithofacies relations in the Late Quaternary Niger delta complex: Sedimentology, v. 21, no. 2, p. 195-222.

Orton, G., and Reading, H., 1993, Variability of deltaic processes in terms of sediment supply, with particular emphasis on grain size: Sedimentology, v. 40, no. 3, p. 475-512.

Paola, C., 2000, Quantitative models of sedimentary basin filling: Sedimentology, v. 47, no. s1, p. 121-178.

-, In Press, A mind of their own: Recent advances in autogenic dynamics in rivers and deltas, in Autogenic Dynamics and Self-Organzation in Sedimentary Systems (In Press), , edited by D. Budd, E. Hajek and S. Purkis: Special Volume of SEPM.

Paola, C., and Martin, J. M., 2012, Mass-balance effects in depositional systems: Journal of Sedimentary Research, v. 82, no. 6, p. 435-450.

Paola, C., Straub, K., Mohrig, D., and Reinhardt, L., 2009, The "unreasonable effectiveness" of stratigraphic and geomorphic experiments: Earth-Science Reviews, v. 97, no. 1, p. 1-43.

Parker, G., 2004, 1D Sediment transport morphodynamics with applications to rivers and turbidity currents, E-book: Saint Anthony Falls Lab., Univ. of Minn., Minneapolis. http://hydrolab. illinois. edu/people/parkerg//morphodynamics_e-book. htm.

Peakall, J., Ashworth, P. J., and Best, J. L., 2007, Meander-bend evolution, alluvial architecture, and the role of cohesion in sinuous river channels: a flume study: Journal of Sedimentary Research, v. 77, no. 3, p. 197-212.

Romans, B. W., Castelltort, S., Covault, J. A., Fildani, A., and Walsh, J., 2015, Environmental signal propagation in sedimentary systems across timescales: Earth-Science Reviews.

Rosen, T., and Xu, Y. J., 2013, Recent decadal growth of the Atchafalaya River Delta complex: Effects of variable riverine sediment input and vegetation succession: Geomorphology, v. 194, p. 108-120.

Sadler, P. M., 1981, Sediment accumulation rates and the completeness of stratigraphic sections: The Journal of Geology, p. 569-584.

Said, R., 2013, The River Nile: geology, hydrology and utilization, Elsevier.

Saller, A., 2003, Sequence stratigraphy and syndepositional tectonics of upper Miocene and Pliocene deltaic sediments, offshore Brunei Darussalam.

Sandal, S. T., 1996, The geology and hydrocarbon resources of Negara Brunei Darussalam, Syabas.

Sheets, B., Hickson, T., and Paola, C., 2002, Assembling the stratigraphic record: Depositional patterns and time‐scales in an experimental alluvial basin: Basin research, v. 14, no. 3, p. 287-301.

Simpson, G., and Castelltort, S., 2012, Model shows that rivers transmit high-frequency climate cycles to the sedimentary record: Geology, v. 40, no. 12, p. 1131-1134.

Slingerland, R., and Smith, N. D., 2004, River avulsions and their deposits: Annu. Rev. Earth Planet. Sci., v. 32, p. 257-285.

Sobel, E. R., and Strecker, M. R., 2003, Uplift, exhumation and precipitation: tectonic and climatic control of Late Cenozoic landscape evolution in the northern Sierras Pampeanas, Argentina: Basin Research, v. 15, no. 4, p. 431-451.

Straub, K. M., and Esposito, C. R., 2013, Influence of water and sediment supply on the stratigraphic record of alluvial fans and deltas: Process controls on stratigraphic completeness: Journal of Geophysical Research: Earth Surface, v. 118, no. 2, p. 625-637.

Straub, K. M., Li, Q., and Benson, W. M., 2015, Influence of sediment cohesion on deltaic shoreline dynamics and bulk sediment retention: A laboratory study: Geophysical Research Letters, v. 42, no. 22, p. 9808-9815.

Straub, K. M., Paola, C., Mohrig, D., Wolinsky, M. A., and George, T., 2009, Compensational stacking of channelized sedimentary deposits: Journal of Sedimentary Research, v. 79, no. 9, p. 673-688.

Straub, K. M., and Wang, Y., 2013, Influence of water and sediment supply on the long‐term evolution of alluvial fans and deltas: Statistical characterization of basin‐filling sedimentation patterns: Journal of Geophysical Research: Earth Surface, v. 118, no. 3, p. 1602-1616.

Strong, N., Sheets, B., Hickson, T., and Paola, C., 2005, A mass-balance framework for quantifying downstream changes in fluvial architecture: Fluvial Sedimentology VII, Special Publication, International Association of Sedimentologists, v. 35, p. 243-253.

Syvitski, J. P., Overeem, I., Brakenridge, G. R., and Hannon, M., 2012, Floods, floodplains, delta plains—a satellite imaging approach: Sedimentary Geology, v. 267, p. 1-14.

Tal, M., and Paola, C., 2007, Dynamic single-thread channels maintained by the interaction of flow and vegetation: Geology, v. 35, no. 4, p. 347-350.

-, 2010, Effects of vegetation on channel morphodynamics: results and insights from laboratory experiments: Earth Surface Processes and Landforms, v. 35, no. 9, p. 1014-1028.

Thomson, D. J., 1982, Spectrum estimation and harmonic analysis: Proceedings of the IEEE, v. 70, no. 9, p. 1055-1096.

Tornqvist, T. E., 1993, Holocene alternation of meandering and anastomosing fluvial systems in the Rhine-Meuse delta (central Netherlands) controlled by sea-level rise and subsoil erodibility: Journal of Sedimentary Research, v. 63, no. 4.

Tucker, G., Lancaster, S., Gasparini, N., and Bras, R., 2001, The channel-hillslope integrated landscape development model (CHILD), Landscape erosion and evolution modeling, Springer, p. 349-388.

Vail, P. R., Mitchum Jr, R., and Thompson III, S., 1977, Seismic Stratigraphy and Global Changes of Sea Level: Part 3. Relative Changes of Sea Level from Coastal Onlap: Section 2. Application of Seismic Reflection Configuration to Stratigrapic Interpretation.

Van De Wiel, M. J., and Coulthard, T. J., 2010, Self-organized criticality in river basins: Challenging sedimentary records of environmental change: Geology, v. 38, no. 1, p. 87-90.

Van Wagoner, J. C., Mitchum, R., Campion, K., and Rahmanian, V., 1990, Siliciclastic sequence stratigraphy in well logs, cores, and outcrops: concepts for high-resolution correlation of time and facies.

von der Heydt, A., Grossmann, S., and Lohse, D., 2003, Response maxima in modulated turbulence. II. Numerical simulations: Physical Review E, v. 68, no. 6, p. 066302.

Wang, X., and Andutta, F., 2013, Sediment transport dynamics in ports, estuaries and other coastal environments, INTECH Open Access Publisher.

Wang, Y., and Evans, M., 1997, Paleomagnetism of Canadian Arctic permafrost; Quaternary magnetostratigraphy of the Mackenzie Delta: Canadian Journal of Earth Sciences, v. 34, no. 2, p. 135-139.

Wang, Y., Straub, K. M., and Hajek, E. A., 2011, Scale-dependent compensational stacking: An estimate of autogenic time scales in channelized sedimentary deposits: Geology, v. 39, no. 9, p. 811-814.

Whipple, K. X., 2001, Fluvial landscape response time: how plausible is steady-state denudation?: American Journal of Science, v. 301, no. 4-5, p. 313-325.

Whipple, K. X., and Tucker, G. E., 1999, Dynamics of the stream‐power river incision model: Implications for height limits of mountain ranges, landscape response timescales, and research needs: Journal of Geophysical Research: Solid Earth, v. 104, no. B8, p. 17661-17674.

-, 2002, Implications of sediment‐flux‐dependent river incision models for landscape evolution: Journal of Geophysical Research: Solid Earth (1978–2012), v. 107, no. B2, p. ETG 3-1-ETG 3-20.

Wickert, A. D., Martin, J. M., Tal, M., Kim, W., Sheets, B., and Paola, C., 2013, River channel lateral mobility: metrics, time scales, and controls: Journal of Geophysical Research: Earth Surface, v. 118, no. 2, p. 396-412.

Willenbring, J. K., Gasparini, N. M., Crosby, B. T., and Brocard, G., 2013, What does a mean mean? The temporal evolution of detrital cosmogenic denudation rates in a transient landscape: Geology, v. 41, no. 12, p. 1215-1218.

Wood, L. J., 2000, Chronostratigraphy and tectonostratigraphy of the Columbus Basin, eastern offshore Trinidad: AAPG bulletin, v. 84, no. 12, p. 1905-1928.

Zagwijn, W., 1989, The Netherlands during the Tertiary and the Quaternary: a case history of coastal lowland evolution, Coastal Lowlands, Springer, p. 107-120.